Department of Applied Mechanics

Effective stiffness and strength properties of cellular materials in the transverse plane

Alp Karakoç

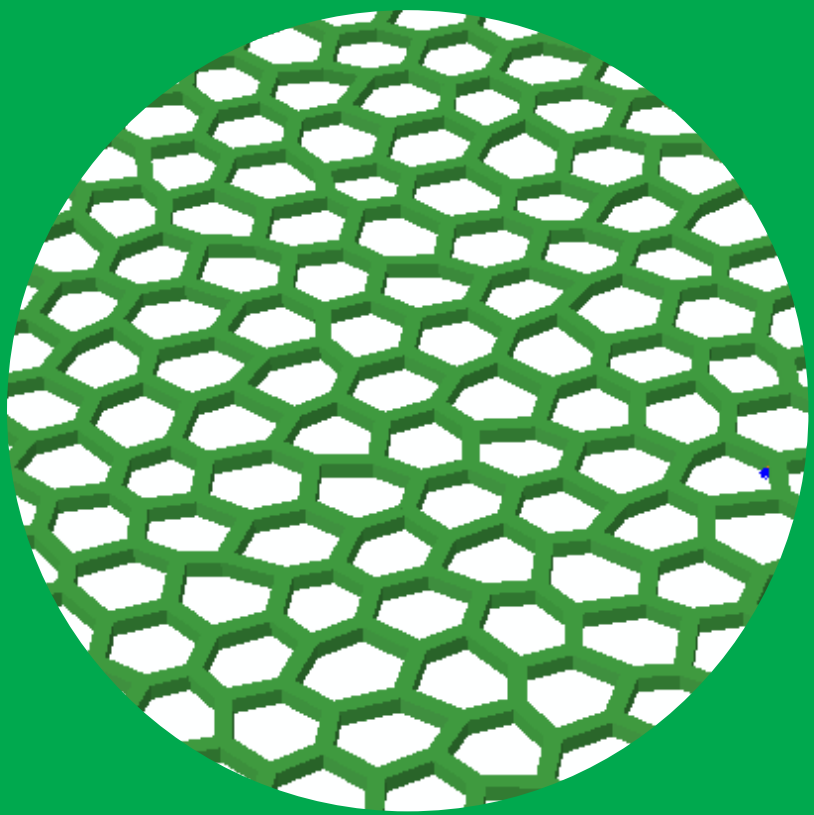

Aalto University

DOCTORAL DISSERTATIONS

Aalto University publication series
DOCTORAL DISSERTATIONS 181/2013

Effective stiffness and strength properties of cellular materials in the transverse plane

Alp Karakoç

A doctoral dissertation completed for the degree of Doctor of Science (Technology) to be defended, with the permission of the Aalto University School of Engineering, at a public examination held at the lecture hall K1/216 of the school on 13th of December, 2013, at 12 noon.

Aalto University
School of Engineering
Department of Applied Mechanics
Mechanics of Materials

Supervising professors
Professor Jukka Tuhkuri
Aalto University, Finland

Thesis advisors
Docent Jouni Freund
Aalto University, Finland

Preliminary examiners
Professor Per Johan Gustafsson
Lund University, Sweden

D.Sc. Lauri Salminen
VTT - Technical Research Center of Finland, Finland

Opponents
Professor Reijo Kouhia
Tampere University of Technology, Finland

Aalto University publication series
DOCTORAL DISSERTATIONS 181/2013

ISBN 978-952-60-5421-6
ISBN 978-952-60-5422-3 (pdf)
ISSN-L 1799-4934
ISSN 1799-4934 (printed)
ISSN 1799-4942 (pdf)
http://urn.fi/URN:ISBN:978-952-60-5422-3

http://lib.tkk.fi/Diss/

Unigrafia Oy
Helsinki 2013

Finland

441 697
Printed matter

Aalto University

Abstract

Aalto University, P.O. Box 11000, FI-00076 Aalto www.aalto.fi

Author
Alp Karakoç

Name of the doctoral dissertation
Effective stiffness and strength properties of cellular materials in the transverse plane

Publisher School of Engineering

Unit Department of Applied Mechanics

Series Aalto University publication series DOCTORAL DISSERTATIONS 181/2013

Field of research Mechanics of Materials

Manuscript submitted 4 April 2013 **Date of the defence** 13 December 2013

Permission to publish granted (date) 21 October 2013 **Language** English

☐ **Monograph** ☒ **Article dissertation (summary + original articles)**

Abstract

In recent years, with growing interest in the energy efficient material processing, and the robust and light-weight product fabrication, cellular materials have found their way into various engineering applications. For the efficient use of these materials, a profound understanding of the relationship between their mechanical and geometrical properties in the transverse plane is necessary. Hence, in order to contribute to the fields of the cellular material modeling and testing, the present study comprising physical and simulation experiments was conducted.

The physical experiments were conducted to determine the effective stiffness properties of the cellular materials in the transverse plane. In these experiments, two different cellular materials, Nomex honeycombs and Norway spruce (Picea abies), were investigated. The experimental data were obtained through the proposed experimental method which involves testing of specimens of different material orientations relative to the loading direction. A benefit of the method is its ability to combine the anisotropic linear elasticity with the physical experiments. Hence, in addition to the effective in-plane elastic moduli and Poisson's ratios, the shear modulus and coefficients of mutual influence characterizing the coupling between the shearing and normal stresses were also determined.

The simulation experiments of the present study were carried out to quantify the effects of the cell geometry, the variations related to the cell wall height and cell wall thickness and the scale on the effective stiffness and strength properties in the transverse plane. For this aim, a statistical simulation model which uses the cell wall mechanical and geometrical properties was introduced. The model was validated through a comparative study based on the results of the physical and simulation experiments on Nomex honeycombs.

The results of the physical and simulation experiments on the effective stiffness properties in the transverse plane imply that the stiffness properties are influenced by the geometrical properties and variations of the cellular structure. Besides, the simulation experiments on the in-plane strength properties reveal that both the scale and cell wall height variations have impact on the cellular material strength.

Keywords Cellular material, transverse plane, Nomex honeycomb, Norway spruce, cell wall height, cell wall thickness, scale, effective stiffness, strength.

ISBN (printed) 978-952-60-5421-6 **ISBN (pdf)** 978-952-60-5422-3

ISSN-L 1799-4934 **ISSN (printed)** 1799-4934 **ISSN (pdf)** 1799-4942

Location of publisher Espoo **Location of printing** Helsinki **Year** 2013

Pages 115 **urn** http://urn.fi/URN:ISBN:978-952-60-5422-3

Preface

The current research study was conducted at the Department of Applied Mechanics, Aalto University. The thesis presents the results of the studies within the research project Energy Efficient Wood Processing and Machining Project (E-wood) supported by Multidisciplinary Institute of Digitalisation and Energy (MIDE) at Aalto University. The financial supports of Ministry of Education of Finland through the National Graduate School in Engineering Mechanics are also acknowledged.

I would like to thank my advisor D.Sc. Jouni Freund and my supervisor Prof. Jukka Tuhkuri for their guidance during my doctoral studies and invaluable comments on the manuscript. The endless support, scientific discussions and encouraging attitude of my senior colleague and lecturer D.Sc. Kari Santaoja are gratefully acknowledged. I would also like to thank Prof. Tapani Vuorinen, Prof. Mark Hughes, Prof. Janne Ruokolainen, and research comrades Johanna Sjölund, Pekka Tukiainen, Mehedi Reza, Iina Solala and Toni Antikainen for their friendship, fruitful discussions and collaborations within the MIDE E-wood research project. The preliminary examiners and the opponent(s) are also greatly acknowledged for their very thorough review. Especially, the valuable comments of the examiners on the need for more careful reporting of the details and limitations are appreciated.

Special thanks go to the previous and current members of the Department of Applied Mechanics at Aalto University, Prof. Grzegorz Glinka, Prof. Gary Marquis, Irina Forsman, Susanna Hurme, Jasmin Jelovica, Jarno Jokinen, Vilho Jussila, Pauliina Kalliala, Olli Kamunen, Kari Kantola, Anssi Karttunen, Niko-Lassi Kurtti, Olli Lassinen, Veijo Laukkanen, Seija Latvala, Pasi Lindroth, Ville Lämsä, Torsten Malm, Seppo Meriläinen, Eeva Mikkola, Mikko Mäkelä, Jairan Nafar Dastgerdi, Ahti Oinonen, Jani Paavilainen, Jani Peltonen, Juhani Pennanen, Arttu Polojärvi, Laura Pyyny, Janne Ranta, Kai Riihinen, Kiran Sahu, Arto Sorsimo, Matyas Taba, Sanna Tossavainen, Raimo von Hertzen and Halid Can Yıldırım, for their friendship and guidance in different stages of the life. I would also like to wish the members of the department the best of luck with their current and future projects and as well as challenges in life.

Finally, I would like to thank my parents, grandparents, relatives, friends and my beloved Linda for their patience and unflagging supports during these years. Now, it is again time for “sailing into dreamland”.

Espoo, 2013
ALP KARAKOÇ

List of publications

This thesis consists of a summary and the following journal articles which were also referred to in the text by their Roman numerals, e.g. Publication I.

I A. Karakoç, J. Freund. Experimental studies on mechanical properties of cellular structures using Nomex honeycomb cores. Composite Structures 2012; 94: 2017-2024.
DOI: 10.1016/j.compstruct.2012.01.024.
Rightslink Printable License Number: 3065300608718.

II A. Karakoç, P. Tukiainen, J. Freund, M. Hughes. Experiments on the effective compliance in the radial-tangential plane of Norway spruce. Composite Structures 2013; 102: 287-293.
DOI: 10.1016/j.compstruct.2013.03.013.
Rightslink Printable License Number: 3131341382365.

III A. Karakoç, K. Santaoja, J. Freund. Simulation experiments on the effective in-plane compliance of the honeycomb materials. Composite Structures 2013; 96: 312–320.
DOI: 10.1016/j.compstruct.2012.09.021.
Rightslink Printable License Number: 3065300104281.

IV A. Karakoç, J. Freund. A statistical failure initiation model for honeycomb materials. Composite Structures 2013; 95: 154-162.
DOI: 10.1016/j.compstruct.2012.07.001.
Rightslink Printable License Number: 3065300779848.

Contribution of the author

Publication I: "Experimental studies on mechanical properties of cellular structures using Nomex honeycomb cores"

The paper presents the physical experiments conducted on Nomex honeycombs to determine the effective stiffness properties in the transverse plane. The author conducted the physical experiments related to the effective stiffness of the artificial cellular material in the transverse plane, analyzed the experiment results and prepared the article manuscript with the co-author.

Publication II: "Experiments on the effective compliance in the radial-tangential plane of Norway spruce"

The paper presents the physical experiments on Norway spruce to determine the effective stiffness properties in the transverse plane. The author analyzed the experiment results related to the effective stiffness of the natural cellular material in the transverse plane and prepared the article manuscript with the co-authors.

Publication III: "Simulation experiments on the effective in-plane compliance of the honeycomb materials"

The paper presents the effects of the cell geometry and the geometrical variations related to the cell wall height and thickness on the effective stiffness properties in the transverse plane by means of the physical and simulation experiments. The author conducted the physical and simulation experiments related to the cellular material effective stiffness in the plane of interest, analyzed the results of both experiments and prepared the article manuscript with the co-authors.

Publication IV: "A statistical failure initiation model for honeycomb materials"

The paper presents the effects of the geometrical variations related to the cell wall height and the scale on the strength properties in the transverse plane by means of the simulation experiments. The author conducted the simulation experiments related to the cellular material strength in the plane of interest, analyzed the experiment results and prepared the article manuscript with the co-author.

Contents

Preface 1

List of publications 3

Contribution of the author 5

Contents 7

1. Introduction 9

1.1 Background 9

1.2 Objectives and limitations 10

1.3 Outline 12

2. Overview of cellular materials 13

2.1 Cellular materials 13

2.2 Effective stiffness and strength 13

2.3 Investigated cellular materials 14

2.3.1 Nomex honeycomb 14

2.3.2 Norway spruce 15

3. Overview of the effective stiffness assessments 19

3.1 General remarks 19

3.2 Effective stiffness properties of cellular materials in the transverse plane 19

3.3 Experimental design and setup 20

3.3.1 Coordinate systems 20

3.3.2 Specimen preparation 20

3.3.3 Test apparatus and measurement domain 22

3.4 Measurement and analysis methods 22

3.4.1 Displacement field 22

3.4.2 Strain and stress measures 23

3.5 Transformation rules for the effective stiffness properties 24

4. Physical experiments on the effective stiffness properties 27

4.1 Nomex honeycomb experiments 27

4.1.1 Experimental design and setup 27

4.1.2 Results and discussions 28

4.2 Norway spruce experiments 31

4.2.1 Experimental design and setup 31

4.2.2 Results and discussions 32

5. Simulation experiments on the effective stiffness properties 35

5.1 Micromechanical model 35

5.1.1 Material element 35

5.1.2 Beam equations 36

5.2 Experimental design and setup 37

5.3 Results and discussions 38

5.3.1 Model validation 38

5.3.2 Effects of the cell wall height and thickness variations ... 39

6. Overview of the strength assessments 43

6.1 Cellular material strength 43

6.2 Strength assessment methods 44

6.2.1 A statistical description for strength through cumulative distribution functions 44

6.2.2 Scale effect on the strength statistics 46

7. Simulation experiments on the strength properties 47

7.1 General remarks 47

7.2 Experimental design and setup 47

7.3 Results and discussions 48

7.3.1 Effects of the cell wall height variations and the scale 49

7.3.2 Statistical strength (failure initiation) model 50

8. Conclusions 55

8.1 Summary and conclusions 55

8.2 Future developments 56

References 59

Publications 67

1. Introduction

1.1 Background

Cellular materials are widely used in a variety of engineering applications such as aviation, automotive, construction and packaging industries because of their physical and mechanical properties including low densities and high stiffness- and strength-to-weight ratios [Evans et al., 1999; Gibson and Ashby, 1999; Hou, 2011; Wadley, 2006; Wang and McDowell, 2004]. Regarding the structural safety, transverse loads in cellular materials should be studied carefully since they can cause irrecoverable problems [Angst-Nicollier, 2012]. For instance, fairly low transverse loads can lead to large local shear strains [Modén, 2008] and collapse of large wooden structures may initiate by transverse failure [Gustafsson, 2003]. Therefore, from the design and modeling aspects of cellular materials, effective stiffness and strength properties in the transverse plane, which is the plane perpendicular to the longitudinal direction of tree trunk [Wiedenhoeft and Miller, 2005] or the plane perpendicular to the thickness direction of honeycomb [Hexcel, 2013], are matters of interest.

Analytical and numerical studies have been performed to estimate the effective stiffness and strength properties of cellular materials in the transverse plane through a description of microstructural properties such as the relative density determining the area fraction in two dimensional structures, the cellular geometry specifying the cell shape, the cellular topology referring to the connectivity of cells, and cell wall material properties [Li et al., 2006; Silva and Gibson, 1997]. These studies include the regular cellular material models, which are based on the analysis of the equilateral cells with identical corner angles [Gibson et al., 1982; Masters and Evans, 1996] and the irregular cellular material models, which take the random shape and size deviations into account [Chen et al., 1999; Chen and Fleck, 2002; Yang and Huang, 2006; Zhu et al., 2001]. In spite of the fact that the relationship between the relative density and the mechanical properties has been carefully scrutinized in these studies, the effects of the cell geometry and its variations still remain poorly comprehended

[Alkhader and Vural, 2008]. In order to understand these effects on the effective stiffness and strength properties in the transverse plane, development of existing cellular material models or introducing new modeling and analysis approaches are thus required.

Physical experiments on the effective stiffness of cellular materials comprise the static and dynamic methods that describe the effective in- and out-of-plane stiffness and strength characteristics and their dependence on the microstructural properties [Balawi and Abot, 2008; Faruggia and Perre 2000; Garab et al., 2010; Gibson and Ashby, 1999; Jernkvist and Thuvander 2001; Kollmann and Côté, 1968; Modén, 2008; Persson, 2000; Schwingschakl et al., 2006]. In most of the physical experiments, uni-axial tension / compression test setups have been successfully used to determine the effective in-plane elastic moduli and the Poisson's ratios. In order to determine the in-plane shear modulus, test setups that are different than uni-axial setups have been proposed in the literature, e.g. notched shear block setup, Iosipescu and Arcan shear test setups [Dahl and Malo, 2009]. If the end-constraint effects of a uni-axial test setup can be reduced, e.g. allowing the rotational degree of freedom of the fixture plates, and specimens can be tested for at least three different material orientations relative to the loading direction, it is also possible to determine all these in-plane stiffness properties by using only one test setup. Furthermore, coefficients of mutual influence characterizing the coupling between the shearing and normal stresses can also be determined in the plane of interest through this approach. This motivates the development and use of uni-axial test setups with rotating upper and lower fixture plates, methods to measure and record the specimen deformation during testing and methods to analyze the test results to determine the effective stiffness properties of cellular materials in the transverse plane.

1.2 Objectives and limitations

The present study focuses on testing and modeling of the effective stiffness and strength properties of cellular materials in the transverse plane. From the material testing point of view, the objectives of the study were:

- To develop a test setup which reduces the end-constraint effects and produces nearly homogeneous stress and strain fields for the use of cellular material testing in the transverse plane;

- To develop non-contacting optical measurement methods and analysis techniques for the physical experiments on the effective in-plane stiffness properties.

From the material modeling point of view, the objectives of the study were:

- To develop a statistical simulation model for conducting simulation experiments on the effective stiffness and strength properties of cellular materials in the transverse plane;

- To validate the proposed statistical simulation model through comparison with the physical experiments on the effective in-plane stiffness properties;

- To study and understand the effects of cell wall height, thickness and scale on the effective in-plane stiffness and strength properties of cellular materials with the validated model;

- To develop a statistical strength model that can estimate the cellular material strength in the normal-shear stress space.

In both the effective in-plane stiffness and strength assessments, following assumptions and limitations were used:

- Reported results describe the local and planar mechanical characteristics of the investigated cellular materials. As an example, specimens were cut from certain growth rings of discs that were sawn from predetermined height of tree trunk. Thus, these results do not try to represent the structural mechanical characteristics of a whole tree trunk.

- Only short-term static testing was taken into consideration. The possible effects of creep and cyclic loads, and the environmental effects such as moisture, temperature were not investigated.

- Effects of defects such as cracks and missing cell walls were not covered.

- The underlying theory to determine the effective stiffness properties in the plane of interest was based on anisotropic linear elasticity. To fulfil the anisotropy, no planes of material symmetry were assigned beforehand.

- Effects of plastic deformations on the material behavior were not covered.

1.3 Outline

The thesis consists of a summary and four original research articles focusing on the effective stiffness and strength properties of cellular materials in the transverse plane and their dependence on the cellular structure.

After this introductory Chapter 1, preliminaries about the mechanics of cellular materials and the investigated materials, Nomex honeycombs and Norway spruce, are presented in Chapter 2. In Chapter 3, theoretical background and investigation methods used to determine the effective stiffness properties of cellular materials in the transverse plane are explained [Publications I, II and III]. In Chapter 4, physical experiments on the effective stiffness properties of the Nomex honeycombs and Norway spruce in the transverse plane are reported [Publications I and II]. In Chapter 5, micromechanical model and simulation experiments on the effective stiffness properties in the transverse plane are discussed [Publication III]. In Chapter 6, strength assessment methods for cellular materials in the transverse plane are discussed [Publication IV]. In Chapter 7, simulation experiments on the cellular material strength in the transverse plane are explained [Publication IV]. Finally, concluding remarks including summary, brief discussions on the results and future work are presented in Chapter 8.

2. Overview of cellular materials

2.1 Cellular materials

Cellular materials are defined as the interconnected network of solid struts or plates that form the edges and faces of cells [Gibson and Ashby, 1999]. Well-known examples of such materials are foams, commercial honeycombs and softwood species, some of which are shown in Fig. 2.1. These materials are used in a wide range of engineering fields because of their favorable physical and mechanical properties [Evans et al., 1999; Yin et al., 2011].

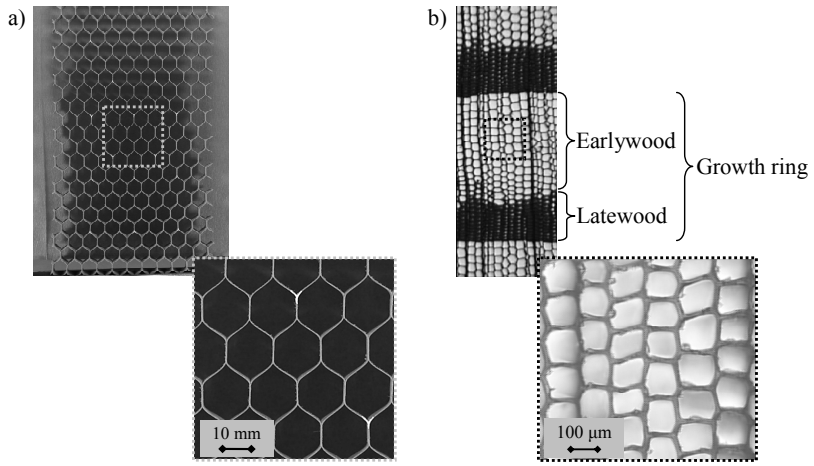

Figure 2.1: Common examples of cellular materials: a) commercial honeycomb and close-up view of its cells and b) softwood and its growth rings consisting of earlywood and latewood.

2.2 Effective stiffness and strength

In cellular material modeling, effective stiffness and strength are of major importance [Hou, 2011]. In a typical material experiment, the first property is obtained through linear elasticity; strictly speaking, the linear relationship between the load and displacement in the range of the proportional limit preserving reversibility. The latter property is determined at the onset of

the irreversible mechanical behavior at the elastic limit depicted in Fig. 2.2. The irreversible material behavior between the elastic and maximum load limits is influenced by microscopic failures and/or plastic deformations [Danielsson, 2009].

As far as the microstructures of the materials in Fig. 2.1 are considered, the effective stiffness is a macroscopic material property representing the behavior of the aggregate, whereas the strength is a microscopic material property describing the behavior of each individual constituent. For cellular materials, both properties are highly dependent on the microscopic properties including the cell shape and connectivity, the cell wall geometrical and mechanical properties and their variations, and the macroscopic properties including the scale [Li et al., 2006; Silva and Gibson, 1997].

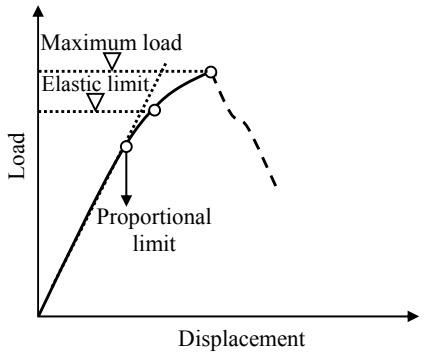

Figure 2.2: Hypothetical load-displacement curve with definitions of the important terms from material modeling point of view [Malvern, 1969; Parnes, 2001]. The dashed line shows a fictive catastrophic regime [Herrmann and Roux, 1990], which was not covered in the present study.

2.3 Investigated cellular materials

In the present study, two different cellular materials, Nomex honeycombs and Norway spruce, were investigated. First, the mechanical properties of the Nomex honeycombs were studied due to their simpler cellular geometries than those of the latter. Then, the experiences and knowledge gained from these studies were transferred to the investigations on the Norway spruce.

2.3.1 Nomex honeycomb

Nomex honeycomb is a commercial material manufactured from aromatic polyamide (aramid) fiber based Nomex paper dipped in phenolic resin.

Nomex paper is produced from two forms of aramid polymer, which are small fibrous binder particles called as fibrids and short aramid fibers cut to length from fiber filaments. These fibers have high thermal resistance, low stiffness and high elongation at room temperature [DuPont-Nomexfiber, 2013].

During the papermaking process, the fibers align themselves with direction of the paper coming off the machine [DuPont-Nomexpaper, 2013]. Thus, Nomex paper has different properties in the (papermaking) machine and cross (-machine) directions [SCAN-test, 1993]. Nomex paper has tensile strength of 86-107 MPa in the machine direction and 38-78 MPa in the cross direction for different thicknesses at room temperature according to ASTM D828-97 test method for tensile properties of paper and paperboard. However, these properties are negatively affected with increasing temperature as specified in the product data sheet [DuPont-Nomexpaper, 2013].

The mechanical characteristics of the Nomex honeycombs arise from both the properties of cell wall material (Nomex paper) and the honeycomb production process as seen in Fig. 2.3 [Bitzer, 1997]. Due to the paper material and geometrical shape of the honeycomb cells, it has high mechanical strength at very low densities and is resistant to corrosion and fire. As a result of these properties, it is extensively used in different structural applications regarding the aviation and automotive industries.

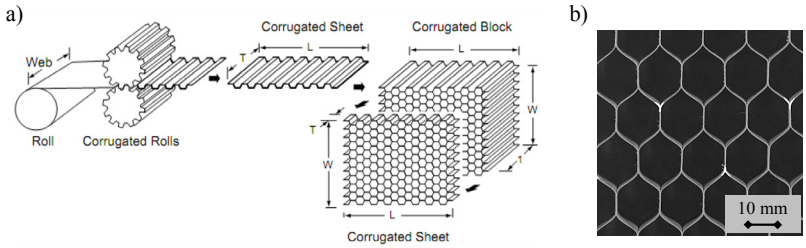

Figure 2.3: Nomex honeycomb: a) the production process, corrugated block and sheet, and b) the material with vertical double walls and inclined single walls in the cross-section perpendicular to the thickness direction *T*, i.e. the transverse plane. Here, *W* and *L* stand for the direction of expansion and the ribbon direction [Hexcel, 2013].

2.3.2 Norway spruce

Norway spruce is a softwood species with needle-like leaves and cones producing and protecting seeds. Differing from hardwood seeds, softwood seeds do not have covering layers [Dahl, 2009]. In addition to this

difference, softwoods also have simpler cellular structure and less geometrical variations within their cells than do hardwoods. Perhaps, the main distinction in terms of the cellular structure is that hardwoods have a characteristic type of cell called as pore (or vessel element) shown in Fig. 2.4, whereas softwoods do not [Wiedenhoeft, 2010].

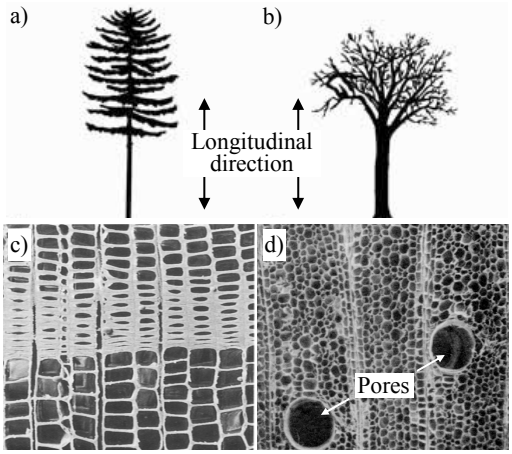

Figure 2.4: Softwoods and hardwoods: a) general structural appearance of a softwood, b) general structural appearance of a hardwood [Wiedenhoeft, 2010], c) cellular structure of Norway spruce (softwood) in the cross-section perpendicular to the longitudinal direction of tree trunk, i.e. the transverse plane [Kahle and Woodhouse, 1994], d) cellular structure of balsa (hardwood) and the pores in the transverse plane [Ashby et al., 1985].

Norway spruce shows a relatively simple structure as it consists of over 85% tracheids and about 7% of ray cells by volume [Persson, 2000; Petric and Ščukanec, 1973]. Tracheids are long tubular cells with hollow centers (lumen) and oriented nearly parallel to the longitudinal direction of tree trunk [Modén, 2008]. As illustrated in Fig. 2.5, tracheids vary in their diameters and wall thicknesses, which are used to distinguish the earlywood and latewood in a softwood growth ring [Havimo et al., 2008]. The diameters of Norway spruce tracheids in early- and latewood vary between 15.0-28.5 μm for juvenile wood (the first 15-20 growth rings from pith seen in Fig. 2.5) and 29.3-39.7 μm for mature wood. The wall thicknesses of the tracheids in early- and latewood are between 0.80-4.60 μm for juvenile wood and 2.10-7.53 μm for mature wood. The lengths of tracheids in early- and latewood are between 1.28-2.70 mm for juvenile wood and 2.80-4.29 mm for mature wood [Brändström, 2001; Persson, 2000].

Tracheids provide mechanical support in the longitudinal direction of tree trunk and serve in the transportation and the storage of water and minerals, while ray cells provide lateral transportation and storage of

biochemicals, and mechanical support in pith-to-bark direction [Persson, 2000; STEP/EUROFORTECH, 1995; Wiedenhoeft and Miller, 2005]. The arrangement of the tracheids and ray cells, the oriented structure of their cell wall layers and the lay-up of the cellulose fibers in these layers contribute to the stiffness and strength properties [Holmberg et al., 1999].

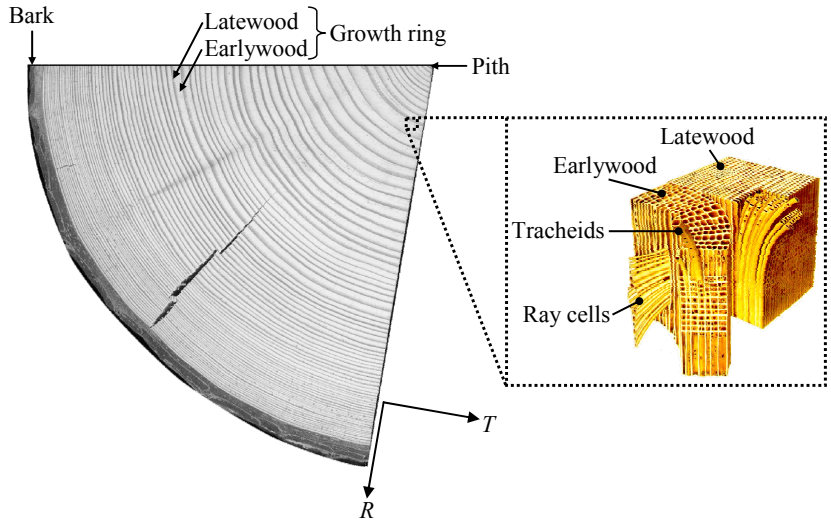

Figure 2.5: Cross-section of a softwood in the transverse plane showing growth rings, pith and bark [Persson, 2000] and schematic representation of the cellular structure including earlywood, latewood, tracheids and ray cells [Bramwell, 1976]. *R* and *T* stand for the radial and tangential directions.

Due to its abundance, favorable physical and mechanical properties, the Norway spruce is one of the most commonly used softwoods in the pulp and paper industries as well as in structural applications such as glue-laminated timber, plywood and particleboard [Garab et al., 2010; Hassel et al., 2009].

3. Overview of the effective stiffness assessments

3.1 General remarks

This chapter describes the effective stiffness properties in the transverse plane and discusses the theoretical background, design, setup and method used in both the physical experiments of Publications I and II and the simulation experiments of Publication III.

The presented experimental method considers a two dimensional plane-stress case. The method should thus be used only in cases, where the response in the investigated plane does not have a significant effect in the third dimension. Even if the method is two dimensional, it can be utilized to study some three dimensional problems. For example, by studying discs of wood from different heights of the tree trunk and keeping track of location and orientation of these discs, the change of in-plane mechanical properties in the longitudinal direction of tree trunk could be measured. However, such a study was not attempted in the present investigations and the emphasis was merely on the development and verification of the experimental method.

3.2 Effective stiffness properties of cellular materials in the transverse plane

Effective stiffness properties of the cellular materials in the transverse plane were quantified in terms of the effective in-plane compliance matrix

$$[\underline{\mathbf{C}}] = \begin{bmatrix} \underline{C}_{11} & \underline{C}_{12} & \underline{C}_{16} \\ \underline{C}_{12} & \underline{C}_{22} & \underline{C}_{26} \\ \underline{C}_{16} & \underline{C}_{26} & \underline{C}_{66} \end{bmatrix} = \begin{bmatrix} 1/E_1 & -\nu_{21}/E_2 & \eta_{12,1}/E_1 \\ -\nu_{12}/E_1 & 1/E_2 & \eta_{12,2}/E_2 \\ \eta_{12,1}/E_1 & \eta_{12,2}/E_2 & 1/G_{12} \end{bmatrix}, \qquad (3.1)$$

in which E_1, E_2, G_{12}, ν_{12}, ν_{21} are the effective elastic moduli, the shear modulus, and the Poisson's ratios, while $\eta_{12,1}$, $\eta_{12,2}$ are the coefficients of mutual influence characterizing the interaction between the shearing and

normal stresses [Lekhnitskii, 1981]. The indices refer to the material 12-coordinate system which is often linked to some geometrical or anatomical features of the material [Jones, 1975]. As illustrated in Fig. 3.1, the material 12-coordinate system was represented with the material *WL*-coordinate system for the Nomex honeycombs and the material *RT*-coordinate system for the Norway spruce in the transverse plane [Publications I, II and III]. *W* and *L* stand for the direction of expansion and the ribbon direction while *R* and *T* stand for the radial and tangential directions. If the axes of the material 12-coordinate system coincide with the material symmetry axes, it serves as the principal material coordinate system and the material is termed orthotropic in the plane of interest, for which the interaction vanishes, i.e. $\eta_{12,1}$, $\eta_{12,2}$ are zeros [Publication III; Tuttle, 2003].

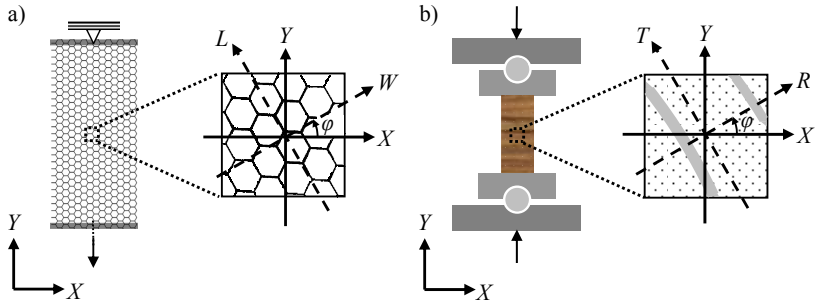

Figure 3.1: Laboratory *XY*- and material *WL*- and *RT*-coordinate systems used in the effective in-plane stiffness experiments: a) Nomex honeycomb specimen [Publication I] and b) Norway spruce specimen (and growth rings as previously depicted in Figs. 2.1 and 2.5) [Publication II]. *W* and *L* stand for the direction of expansion and the ribbon direction while *R* and *T* stand for the radial and tangential directions. φ is the (counterclockwise) material orientation angle between the laboratory and material coordinate systems.

3.3 Experimental design and setup

3.3.1 Coordinate systems

In the experiments on the effective stiffness of Nomex honeycombs and Norway spruce in the transverse plane, two coordinate systems were used by taking directional dependence of the mechanical properties into account. As seen in Fig. 3.1, these coordinate systems were specified with the laboratory *XY*- and material 12-coordinate systems, where the latter was represented as the material *WL*-coordinate system for Nomex honeycombs and material *RT*-coordinate system for Norway spruce.

3.3.2 Specimen preparation

Specimen preparation is illustrated in Fig. 3.2. First, material sheets were prepared. Only one material sheet was used for studying the effective in-

plane stiffness properties of each Nomex honeycomb sample. On the other hand, it was possible to use several material sheets in Norway spruce experiments because the upper and lower material sheet surfaces were readily defined. Here, a sample was defined as the set of specimens with the same geometrical properties, e.g. the same cell size and thickness in case of Nomex honeycombs.

The material 12-coordinate system was specified on material sheets and was roughly aligned with the geometrical symmetry axes for simplicity. For Nomex honeycombs, dashed lines were drawn along the direction of expansion *W* and straight lines were drawn along the ribbon direction *L* on only one surface of each honeycomb material sheet. In case of Norway spruce experiments, the coordinate system was specified along the radial direction *R* and tangential direction *T* on only one surface of each wood material sheet. Thereafter, specimens were cut out from the material sheet based on the dimensions and orientations, which were determined during the design stage of the experiments. The orientations were defined with the (counterclockwise) material orientation angles φ between the laboratory *XY*- and material 12-coordinate systems.

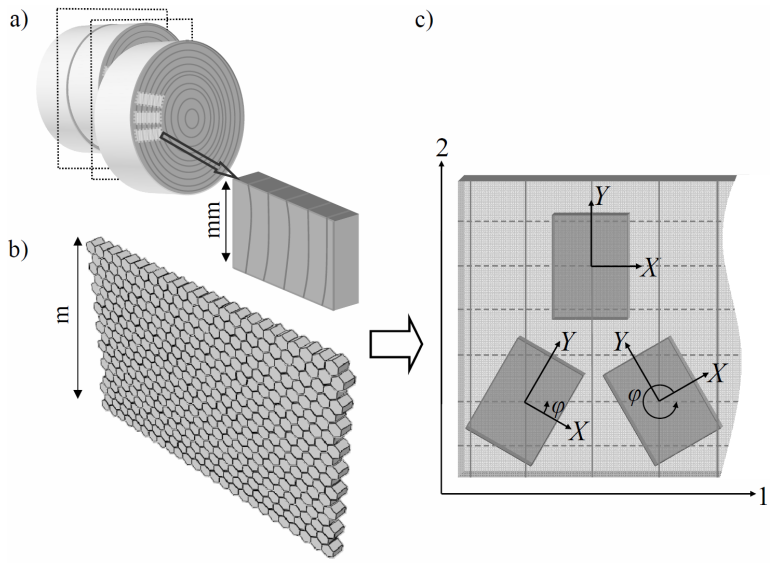

Figure 3.2: Schematic representation of specimen preparation: a) Norway spruce material sheet cut out from wood disc (dimensions in order of millimetres), b) Nomex honeycomb material sheet (dimensions in order of meters) and c) specimens taken out from the material sheet. The dashed horizontal lines on the sheet represent the 1st material direction and the solid vertical lines represent the 2nd material direction. φ is the (counterclockwise) material orientation angle between the laboratory and material coordinate systems.

3.3.3 Test apparatus and measurement domain

The aim in designing the test apparatuses was to reduce the effects of boundary artifacts, which causes non-uniform deformation [Marin et al., 2002]. This was done by allowing rotational degree of freedom of the fixture plates [Publications I, II and III], which reduces the end-constraint effects, e.g. shear at the boundary extremes of the specimen [Xiao et al., 2011]. In addition to this, measurement domain Ω_m was chosen to be smaller than the entire specimen so as to eliminate the undesired artifacts on the experiment results. Hence, the measurements were solely performed inside Ω_m shown in Fig. 3.3.

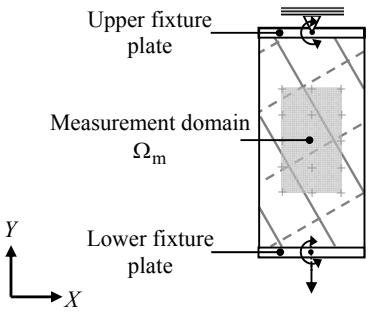

Figure 3.3: Schematic representation of the experiment setup and measurement domain Ω_m formed with markers "+".

3.4 Measurement and analysis methods

3.4.1 Displacement field

Three different measurement techniques were used to determine the displacement field inside the measurement domain Ω_m illustrated in Fig. 3.3. In Publication I, marker tracking technique was introduced for the displacement field measurements of honeycomb specimens. In this technique, Ω_m was defined with the markers drawn on the predetermined cell vertices of the honeycomb specimens and positions of these markers were tracked during testing. In Publication II, digital image correlation was used for measuring the displacement field of spruce specimens and Ω_m was formed with virtual markers called as subset centers. In Publication III, displacement field was computed by tracing and monitoring the positions of the vertex points forming Ω_m.

In all these approaches, the positions (X_i^f, Y_i^f) for $i \in \{1, 2, ..., m\}$ tracking points associated to the frame (or time instant) f were first determined. Then, the displacements were calculated through

$$\begin{Bmatrix} u_{Xi}^f \\ u_{Yi}^f \end{Bmatrix} = \begin{Bmatrix} X_i^{f+1} - X_i^f \\ Y_i^{f+1} - Y_i^f \end{Bmatrix}, \tag{3.2}$$

in which u_{Xi}, u_{Yi} are the displacement components in the directions of the X- and Y-axes, respectively. The displacements of Eq. (3.2) were considered as the values of the continuous linear displacement field $\vec{u}^f$. In the component form,

$$\begin{Bmatrix} u_X^f \\ u_Y^f \end{Bmatrix} = \begin{bmatrix} p_1^f & p_2^f & p_3^f \\ p_4^f & p_5^f & p_6^f \end{bmatrix} \begin{Bmatrix} 1 \\ X \\ Y \end{Bmatrix}, \tag{3.3}$$

for which p_j^f for $j \in \{1, 2, ..., 6\}$ are the polynomial coefficients. Since a homogeneous strain field was considered in the measurement domain, only the first order polynomials were used. The values of p_j^f for $j \in \{1, 2, ..., 6\}$ were calculated as the unique minimizer of the least squares function

$$\pi(p_1^f, p_2^f, \ldots) = \sum_{i=1}^{n} \left\| \begin{Bmatrix} u_{Xi}^f \\ u_{Yi}^f \end{Bmatrix} - \begin{bmatrix} p_1^f & p_2^f & p_3^f \\ p_4^f & p_5^f & p_6^f \end{bmatrix} \begin{Bmatrix} 1 \\ X_i^f \\ Y_i^f \end{Bmatrix} \right\|^2, \tag{3.4}$$

in which the summation $\sum$ is over n points and the matrix norm $\| \ \|$ is the Euclidean. The polynomial coefficients were separately calculated for each frame. Hereafter, superscript f is omitted to simplify the notation.

3.4.2 Strain and stress measures

Once $\vec{u}$ of Eq. (3.3) was calculated, the components of the small strain tensor **e** were determined as follows

$$\begin{Bmatrix} e_{XX} \\ e_{YY} \\ 2e_{XY} \end{Bmatrix} = \begin{Bmatrix} \partial u_X / \partial X \\ \partial u_Y / \partial Y \\ \partial u_X / \partial Y + \partial u_Y / \partial X \end{Bmatrix}. \tag{3.5}$$

Stress tensor **s** was calculated through the measured load, cross-sectional area and normal vectors under the assumption of small strains.

3.5 Transformation rules for the effective stiffness properties

In the laboratory *XY*-coordinate system depicted in Fig. 3.3, the linear stress-strain relationship was expressed using the Voigt notation

$$\{\mathbf{e}\} = [\mathbf{C}]\{\mathbf{s}\}, \tag{3.6}$$

in which $\{\mathbf{e}\}$ and $\{\mathbf{s}\}$ are the column vector representations for the strain and stress tensors with the assumption of symmetry, whereas $[\mathbf{C}]$ is the square matrix representation for the fourth-order compliance tensor $\mathbf{C}$. Here, it should be noted that $[\mathbf{C}]$ of Eq. (3.6) denotes the effective in-plane compliance matrix in the laboratory *XY*-coordinate system, which is different from $[\underline{\mathbf{C}}]$ of Eq. (3.1) denoting the effective in-plane compliance matrix in the material 12-coordinate system. Then, Eq. (3.6) was expanded to the component form as

$$\begin{Bmatrix} e_{XX} \\ e_{YY} \\ 2e_{XY} \end{Bmatrix} = \begin{bmatrix} C_{11} & C_{12} & C_{16} \\ C_{12} & C_{22} & C_{26} \\ C_{16} & C_{26} & C_{66} \end{bmatrix} \begin{Bmatrix} s_{XX} \\ s_{YY} \\ s_{XY} \end{Bmatrix} = [\mathbf{T}]^{\mathrm{T}} \begin{bmatrix} \underline{C}_{11} & \underline{C}_{12} & \underline{C}_{16} \\ \underline{C}_{12} & \underline{C}_{22} & \underline{C}_{26} \\ \underline{C}_{16} & \underline{C}_{26} & \underline{C}_{66} \end{bmatrix} [\mathbf{T}] \begin{Bmatrix} s_{XX} \\ s_{YY} \\ s_{XY} \end{Bmatrix}, \tag{3.7}$$

in which the compliance symmetry is taken into account. Thus, the number of the independent parameters reduces to 6 [Kaw, 2006]. In Eq. (3.7), superscript T denotes the matrix transpose and $[\mathbf{T}]$ is the transformation matrix. According to [Jones, 1975],

$$[\mathbf{T}] = \begin{bmatrix} \cos^2\varphi & \sin^2\varphi & 2\sin\varphi\cos\varphi \\ \sin^2\varphi & \cos^2\varphi & -2\sin\varphi\cos\varphi \\ -\sin\varphi\cos\varphi & \sin\varphi\cos\varphi & \cos^2\varphi - \sin^2\varphi \end{bmatrix} \tag{3.8}$$

where φ is the (counterclockwise) material orientation angle between the laboratory and material coordinate systems.

Transformation rules in Eqs. (3.7) and (3.8) are used to express $[\mathbf{C}]$ of any rotated coordinate system in terms of $[\underline{\mathbf{C}}]$ in the basis of the material coordinate system. The values of $\underline{C}_{11}, \ldots, \underline{C}_{66}$ can be obtained by using three linearly independent homogeneous stress states $s^i_{XX}, s^i_{YY}, s^i_{XY}$ for $i \in \{1, 2, 3\}$. Assuming that the corresponding strain components $e^i_{XX}, e^i_{YY}, e^i_{XY}$ are measured in some manner,

$$[\underline{\mathbf{C}}] = \left[\begin{array}{c|c|c} e^1_{XX} & e^2_{XX} & e^3_{XX} \\ e^1_{YY} & e^2_{YY} & e^3_{YY} \\ 2e^1_{XY} & 2e^2_{XY} & 2e^3_{XY} \end{array}\right] \left[\begin{array}{c|c|c} s^1_{XX} & s^2_{XX} & s^3_{XX} \\ s^1_{YY} & s^2_{YY} & s^3_{YY} \\ s^1_{XY} & s^2_{XY} & s^3_{XY} \end{array}\right]^{-1}. \tag{3.9}$$

However, in order to reduce the random measurement errors, specimens were tested for more than three different material orientations relative to the loading direction. Then, the parameters were calculated as the unique minimizer of the least squares function

$$\pi(\underline{C}_{11},..,\underline{C}_{66}) = \sum_{i=1}^{n} \left\| \begin{Bmatrix} e_{XX}^i \\ e_{YY}^i \\ 2e_{XY}^i \end{Bmatrix} - [\mathbf{T}]^{\mathrm{T}} \begin{bmatrix} \underline{C}_{11} & \underline{C}_{12} & \underline{C}_{16} \\ \underline{C}_{12} & \underline{C}_{22} & \underline{C}_{26} \\ \underline{C}_{16} & \underline{C}_{26} & \underline{C}_{66} \end{bmatrix} [\mathbf{T}] \begin{Bmatrix} s_{XX}^i \\ s_{YY}^i \\ s_{XY}^i \end{Bmatrix} \right\|^2, \quad (3.10)$$

in which the matrix norm $\| \ \|$ is the Euclidean and n is the number of tested specimens.

The abovementioned methodology formed the theoretical basis of the investigations on the effective stiffness properties of the cellular materials in the transverse plane. It was used in both the present physical and simulation experiments to determine the effective in-plane elastic moduli, Poisson's ratios, shear modulus and coefficients of mutual influence characterizing the coupling between shearing and normal stresses.

4. Physical experiments on the effective stiffness properties

4.1 Nomex honeycomb experiments

4.1.1 Experimental design and setup

Uni-axial tension experiments were conducted on the Nomex honeycomb specimens as shown in Fig. 4.1. Specimens of different material orientations $\varphi \in \{0^\circ, 45^\circ, -45^\circ, 90^\circ\}$ were cut out from the material sheets with cell size $c \in \{5, 6, 13\}$ mm and thickness $\mathcal{T} \in \{7, 12\}$ mm. Specimen width and length were decided to be $\mathcal{W}$≈150 mm and $\mathcal{L}$≈300 mm by following the ASTM C363 test method for sandwich constructions and cores [MIL-STD-401B, 1967]. For each material orientation φ, two specimens were prepared. In other words, 8 specimens were tested to determine the effective in-plane stiffness properties of each sample designated with S-c-$\mathcal{T}$.

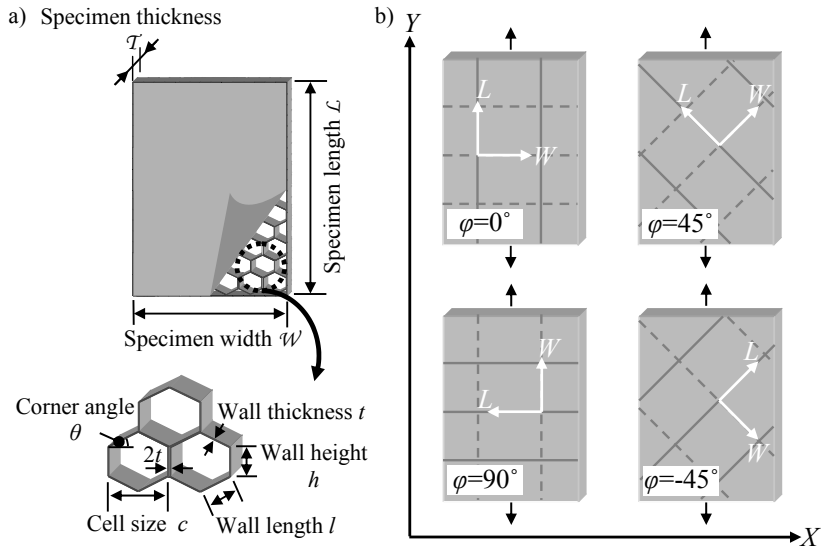

Figure 4.1: Nomex honeycomb specimens: a) schematic representation of the specimen geometry and b) schematic representation of specimens with different material orientations relative to uni-axial tensile loading.

The experiments were conducted in a steel frame as shown in Fig. 4.2. In this setup, the upper and lower boundary extremes of the specimen were glued to the fixture plates that were connected to the joints on the frame. The lower joint was a stationary pin joint with the rotational degree of freedom around the *XY*-plane normal vector. The upper joint was adjusted to move upwards and downwards along the *Y*-axis and to rotate around the *XY*-plane normal vector.

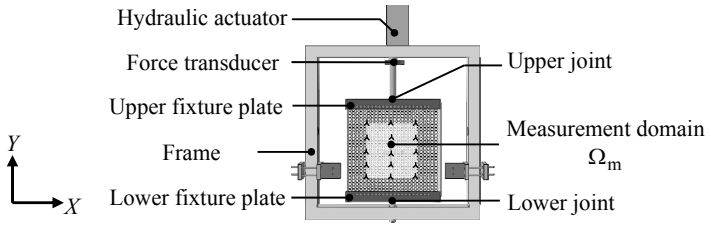

Figure 4.2: Schematic representation of the uni-axial tensile experiment setup: the frame, the fixture plates, the joints and the measurement domain Ω_m defined with the markers.

During these experiments, load $\underline{F}$ was measured with the force transducer and the marker position data was measured with the marker tracking technique. The position data were used to determine the displacement field inside the measurement domain Ω_m of Fig. 4.2, which was smaller than the entire domain (specimen). As a result of the boundary conditions and Ω_m, the effects of the boundary artifacts on the test results were aimed to be reduced.

4.1.2 Results and discussions

Cell wall deformation started with cell wall bending, which is assumed to be the dominant mechanism in the linear elastic region [Chen et al., 2009; Gibson and Ashby, 1999]. In the literature, this mechanism is explained in terms of cell walls loaded in bending so that their ends are constrained not to rotate [Andrews et al., 1999]. Under the effect of this mechanism, inclined cell walls were observed to take the form of S-shaped curves, which can be seen in Figs. 4.3 and 4.4. Densification, during which opposing cell walls contact each other [Gibson and Ashby, 1999], and debonding, during which adjacent cell walls separate from each other along their interface zones (glue lines) [Dill-Langer et al., 2002], were other possible active mechanisms in the following stages of the experiments. However, these two latter mechanisms were not covered in the present effective in-plane stiffness analysis.

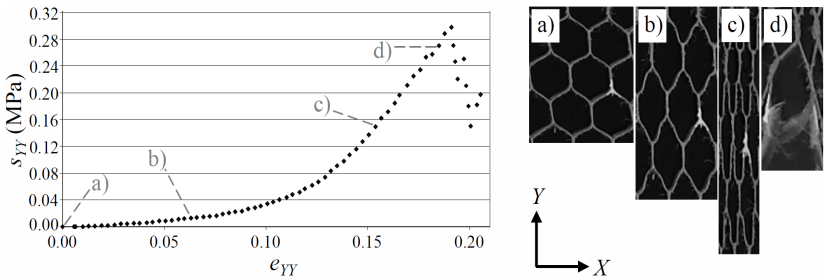

Figure 4.3: Measured strain e_{YY} as a function of nominal stress s_{YY} (load/initial area) for a Nomex honeycomb specimen with cell size c=6 mm, specimen thickness $\mathcal{T}$=7 mm and material orientation angle φ=0° under the uni-axial tensile load along the Y-axis: a) undeformed specimen, b) cell wall bending, c) densification and d) debonding.

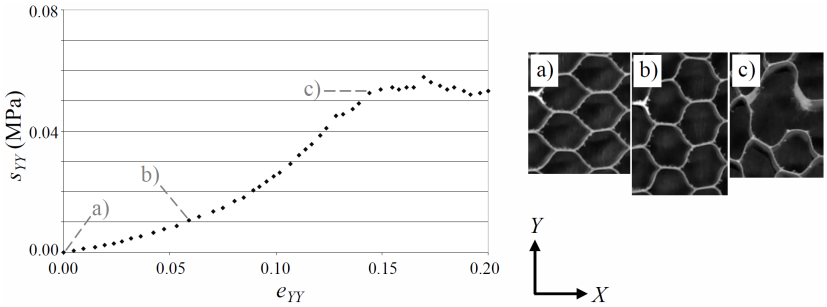

Figure 4.4: Measured strain e_{YY} as a function of nominal stress s_{YY} (load/initial area) for a Nomex honeycomb specimen with cell size c=6 mm, specimen thickness $\mathcal{T}$=7 mm and material orientation angle φ=90° under the uni-axial tensile load along the Y-axis: a) undeformed specimen, b) cell wall bending and c) debonding.

Since the main purpose was to measure the effective in-plane stiffness, the investigations were limited to the linear elastic region that was defined based on the measured strain values. The strain value at the upper limit of the linear elastic region was taken to be ~25% of the strain value measured at the maximum nominal stress s_{YY}, e.g. e_{YY}=0.048 at the upper limit of the linear elastic region in Fig. 4.3. The results obtained from the physical experiments [Publication I] were compared with the ones calculated from the analytical solution based on the bending deformation of the cell walls [Gibson and Ashby, 1999]. This comparison was used to (1) analyze the effects of the geometrical properties on the effective in-plane stiffness and (2) to seek the possibility of building a more comprehensive model based on the beam theory.

Table 4.1 tabulates the comparison of the measured and analytical values for the Nomex honeycomb samples in the material *WL*-coordinate system. The cell wall elastic modulus E_s=7.9 GPa [Publication I] and the samples were designated with S-c-$\mathcal{T}$, for which the cell sizes were $c \in${5, 6, 13} mm and the specimen thicknesses were $\mathcal{T} \in${7, 12} mm.

Table 4.1: The geometrical and effective stiffness properties of the Nomex honeycomb samples in the transverse plane. Prefix An- stands for the calculated values based on the analytical solution as provided in [Gibson and Ashby, 1999; Publication I].

Sample	$h(\sim l)$ (mm)	t (mm)	θ (°)	E_W (kPa)	E_L (kPa)	G_{WL} (kPa)	ν_{WL}	ν_{LW}	$-\eta_{WL,W}$	$-\eta_{WL,L}$
S-5-7	2.5	0.05	32	121.0	158.5	92.6	1.12	1.47	0.019	-0.103
An-S-5-7				124.1	157.7	90.7	0.89	1.13	---	---
S-5-12	2.5	0.05	34	105.8	159.8	98.3	0.97	1.47	-0.049	0.004
An-S-5-12				106.9	172.0	94.6	0.79	1.27	---	---
S-6-7	3.2	0.06	26	171.9	118.0	64.3	1.31	0.89	-0.048	0.077
An-S-6-7				168.4	102.6	66.3	1.28	0.78	---	---
S-6-12	3.2	0.06	28	150.0	105.7	71.4	1.29	0.91	-0.104	-0.075
An-S-6-12				141.2	110.6	69.0	1.13	0.88	---	---
S-13-7	6.6	0.13	32	122.9	154.2	91.9	1.26	1.58	0.073	-0.069
An-S-13-7				118.5	150.6	86.7	0.88	1.13	---	---
S-13-12	6.8	0.13	32	96.5	128.2	84.6	0.91	1.21	0.004	0.024
An-S-13-12				108.4	137.7	79.2	0.88	1.13	---	---

As Table 4.1 shows, the measured coefficients of mutual influence $\eta_{WL,W}$, $\eta_{WL,L}$ were low, which implies weak interaction between the shearing and normal stresses in relation to $\eta_{ij,i}=2e_{ij}/e_i$ for $i, j \in \{W, L\}$ [Mascia and Vanalli, 2012]. It can be deduced that the axes of the material *WL*-coordinate system were almost aligned with the material symmetry axes and the material *WL*-coordinate system served as the principal material coordinate system. Table 4.1 also shows the dominant effect of the corner angle θ on the effective compliance. The comparison between the same cell size samples S-5-7 and S-5-12 or S-6-7 and S-6-12 show that E_W and ν_{WL} were inversely proportional to θ for the measured angle range, which is mainly related to the contribution of the inclined cell walls [Balawi and Abot, 2008]. In addition to this, when θ had greater value than 30°, more material was oriented along the ribbon direction *L*. Therefore, the material became stiffer along this direction, which resulted in $E_L>E_W$ for $\theta>30°$ and $E_L<E_W$ for $\theta<30°$. Similar trend was valid for the Poisson's ratios ν_{WL} and ν_{LW}, which can be attributed to the reciprocal relation $\nu_{WL}E_L=\nu_{LW}E_W$ [Jones, 1975]. On the other hand, it was very difficult to analyze the individual effects of the cell wall thickness t and height h. However, their combined effect t/h shows that when t/h decreased and the cell walls became more slender, the cell walls were less resistant to the deformation. This effect can be seen when comparing the results of the samples S-13-7 and S-13-12 in Table 4.1, where all moduli decrease with a decrease in t/h. In addition to these, the effect of the specimen thickness $\mathcal{T}$ was investigated but its effect was negligible compared to the dominant effects of θ and t/h.

The comparison of the values in Table 4.1 indicates that the maximum relative error between the measured and modeled values was 28.0% for ν_{LW} of the sample S-13-7, whereas the minimum relative error was 0.5% for E_L of the sample S-5-7. This shows that the analytical model based on the beam theory [Gibson and Ashby, 1999] estimated the effective in-plane stiffness properties within reasonable accuracy. Thus, a more comprehensive model was aimed to be built to determine the values within higher accuracy.

4.2 Norway spruce experiments

4.2.1 Experimental design and setup

Uni-axial compression experiments were conducted on the Norway spruce specimens with 7 different material orientations relative to the loading direction as shown in Fig. 4.5. For each material orientation, i.e. $\varphi \in \{0^\circ, 15^\circ, 30^\circ, 45^\circ, 60^\circ, 75^\circ, 90^\circ\}$, 10 specimens were prepared (the growth ring numbers 18-25 with the radial distance of 50-80 mm from the pith of the disc), where the cross-sectional dimensions were 15 mm × 5 mm in the material *RT*-coordinate system and the thickness was 5 mm in the longitudinal direction. Hence, in total, 70 specimens were prepared and tested. As shown in Fig. 4.6, specimens were covered with an arbitrary speckle patterns for the optimal use of the digital image correlation in the displacement field measurements [Publication II].

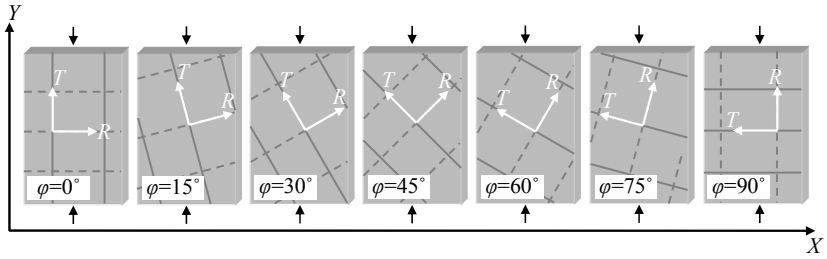

Figure 4.5: Schematic representation for specimens with different material orientations relative to uni-axial compressive loading.

During these experiments, position data of the subset centers of the speckle patterns were obtained with the digital image correlation and load $\underline{F}$ was measured through the force transducer. The position data were used to determine the displacement field inside the measurement domain Ω_m shown in Fig. 4.6.

In order to provide appropriate condition for the uni-axial loading, the upper and lower cross-heads of the loading stage shown in Fig. 4.6 were adjusted to move along the *Y*-axis whilst the rotational degree of freedom was given with the additional steel cylinders between the cross-heads and the fixture plates. Under this gripping condition, the likely effect of shear at the boundary extremes was aimed to be reduced.

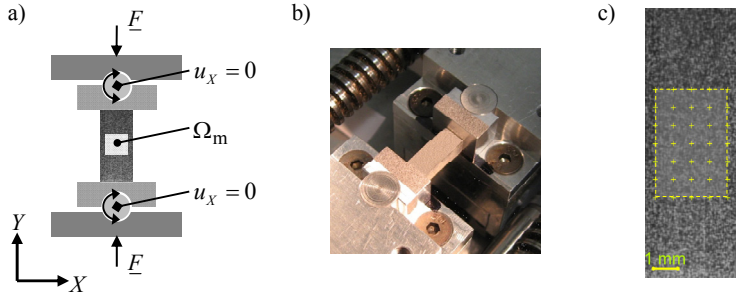

Figure 4.6: Experiment setup: a) schematic representation of the loading and boundary conditions, and the measurement domain Ω_m, b) the loading stage, c) the specimen with the speckle pattern and the measurement domain Ω_m defined with the subset centers. Here, u_X is the displacement component in the direction of the *X*-axis.

4.2.2 Results and discussions

The proposed experimental method and the knowledge gained from the physical experiments on the Nomex honeycombs were used to obtain the effective stiffness properties of the Norway spruce in the transverse plane. The results were then compared with the literature values (1) to understand the trends among the effective in-plane stiffness properties and (2) to examine and verify the proposed method.

Stress-strain relationship was determined for different measurement domains so as to identify the measurement domain, for which the effects of boundary artifacts were minimized. The stress-strain curves for the material orientation angle φ=45° are shown in Fig. 4.7. Two measurement domains that were approximately 6.3 mm × 4.5 mm (280 pixels × 200 pixels) (Domain 1) and 13.5 mm × 4.5 mm (600 pixels × 200 pixels) (Domain 2) were taken into account. It was observed that there were slight differences between the strain measurements over these domains. To ensure a safe procedure, it was proposed to confine the measurements on the smaller domain [Publication II].

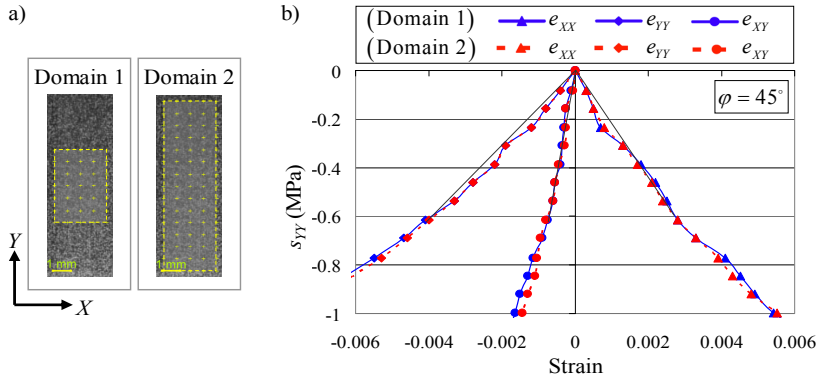

Figure 4.7: Measured strain components as a function of nominal stress s_{YY} (load/initial area) under the uni-axial compressive load along the *Y*-axis: a) predetermined measurement domains on the speckle patterns and b) the stress-strain curves for a specimen with the material orientation angle φ=45°. Solid lines were plotted to indicate the linear stress-strain relationship [Publication II].

Although the experiments were carried out till the specimen failure, the region of interest was the linear elastic part of the stress-strain curves to determine the effective stiffness properties of Norway spruce in the transverse plane, which is listed in Table 4.2. The measured values were compared with the ones obtained for similar densities in the literature.

Table 4.2: The effective stiffness properties of the Norway spruce in the transverse plane based on Publication II, survey-I [Kahle and Woodhouse, 1994], survey-II [Carrington, 1923], survey-III [Kollman and Côté, 1968].

	Density (g/cm³)	E_R (MPa)	E_T (MPa)	G_{RT} (MPa)	ν_{RT}	ν_{TR}	$-\eta_{RT,R}$	$-\eta_{RT,T}$
Present study	0.39-0.44	955	411	25	0.62	0.27	0.094	0.061
Survey-I	0.37-0.55	640-890	360-630	22-37	0.43-0.64	0.25-0.33	---	---
Survey-II	0.39	640	420	26	0.64	0.32	---	---
Survey-III	0.44-0.50	690-810	390-630	35-36	0.42-0.43	0.24-0.33	---	---

The comparison between the values in Table 4.2 shows that the measured data in the present study were in the range determined by the previous studies. However, the values provided in the literature spreads over a wide range, which can be due to the intrinsic properties of the investigated tree trunk, selection of the specimens from different radial positions in the growth ring, and the specimen dimensions. In addition to the structural variations, the measurement and analysis techniques of the conventional experiments, e.g. strain gauges and linear variable differential transformer

LVDT, could be the other possible factors affecting the results [Publication II].

Despite the differences in both the measured and literature data of Table 4.2, the trend between the elastic moduli E_R, E_T in the radial R and the tangential T directions, i.e. $E_R > E_T$, was obvious. Higher material stiffness along the R direction was possibly due to the cell tessellation affecting the cell wall deformation mechanisms and the radial alignment of the ray cells acting as barrier against the radial deformation [Alkhader and Vural, 2008; Deshpande et al., 2001; Kahle and Woodhouse, 1994; Persson, 2000]. There was a similar trend between the Poisson's ratios ν_{RT} and ν_{TR}, i.e. $\nu_{RT} > \nu_{TR}$, as also pointed out in Publication II. In addition to these, values for the coefficients of mutual influence $\eta_{RT,R}$, $\eta_{RT,T}$ indicates that there was weak coupling between the shearing and normal stresses in the plane of interest. It can be thus deduced that the selected material RT-coordinate system served as the principal material coordinate system.

5. Simulation experiments on the effective stiffness properties

5.1 Micromechanical model

In order to compute the mechanical properties of cellular materials, various studies have been conducted in which the main strategy is based on continuum or micromechanical models. In continuum models, material details and microscopic heterogeneities, e.g. geometrical and mechanical properties of constituents and their variations, are averaged over the representative volume elements RVEs [Landis et al., 2002]. The accuracy in continuum models is dependent on the selected RVE size and how well the material details are approximated and represented with these RVEs [Nemat-Nasser and Hori, 1999; Ren and Zheng, 2002]. Therefore, continuum models are safely used in the analyses for which the material details do not have the highest priority. In micromechanical models, geometrical and mechanical properties are modeled for each constituent separately, which increases the computational cost. However, it is possible to determine the stresses and strains in each constituent accurately [Kumar and McDowell, 2004]. Thus, the properties of the material and its constituents can be directly related to each other in micromechanical models [Aboudi, 1995].

In the present study, micromechanical modeling approach was selected due to its convenience in associating the cell wall properties with the effective stiffness and strength properties in the transverse plane. For this purpose, two dimensional cellular materials were modeled with beam networks representing the heterogeneous nature of cellular materials [Publications III and IV].

5.1.1 Material element

As seen in Fig. 5.1, the material element used in the simulation experiments was a hexagonal cellular structure within the domain of width W and length

$\mathcal{L}$. The domain was composed of two sub-domains which were the solution domain Ω and the boundary domain $\partial\Omega$. The solution domain was composed of the vertices and the centerlines of the cell walls modeled as beams, whereas the boundary domain $\partial\Omega$ was composed of vertices. The vertex points at these sub-domains were distinguished by means of their connectivity. If a vertex point was common to three adjacent cell walls, it had connectivity three and belonged to the solution domain Ω. Otherwise, it was part of the boundary domain $\partial\Omega$.

The material element geometry was described with the cell size c, the corner angle θ, the cell wall height h and thickness t, and the specimen thickness $\mathcal{T}$, width $\mathcal{W}$ and length $\mathcal{L}$ as previously depicted in Fig. 4.1. In the simulation experiments, h and t were taken as statistical quantities defined with their mean values h_{mean}, t_{mean} and standard deviations h_{stdev}, t_{stdev}. The bounds of the geometrical irregularities were described with the coefficient of variation terms, i.e. the variation term for cell wall height $\alpha=h_{\text{stdev}}/h_{\text{mean}}$ and the variation term for cell wall thickness $\beta=t_{\text{stdev}}/t_{\text{mean}}$. For example, $\alpha=0$ corresponds to a regular cell geometry with the cell wall height h^0 and $\alpha>0$ corresponds to an irregular cell geometry as illustrated in Fig. 5.1 [for details, see Publication III].

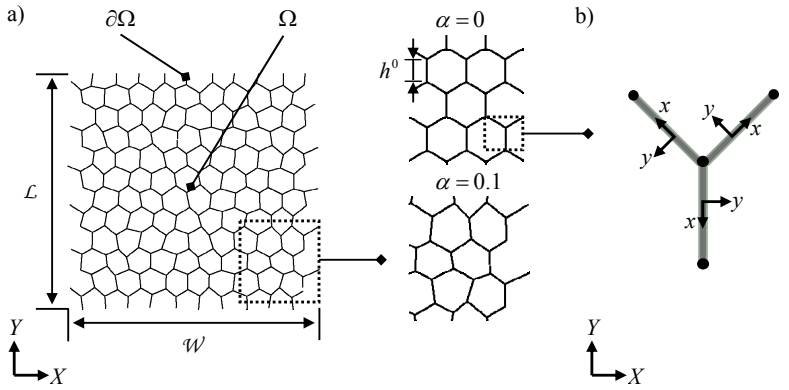

Figure 5.1: Material element: (a) the solution domain Ω, the boundary domain $\partial\Omega$, and illustration of the regular and irregular cell geometries, (b) the beam xy-coordinate system.

5.1.2 Beam equations

In the micromechanical model, cell walls of the material element were modeled as elastic Bernoulli beams. The possible material inside the cells, e.g. (possible) air and water content in the tested honeycomb and softwood specimens, was assumed to be much softer than that of the cell walls, thus

its influence on the mechanical response was neglected. The component form of the equilibrium equations in the beam *xy*-coordinate system of Fig. 5.1 was as follows

$$\begin{Bmatrix} E_s A u_x'' \\ -E_s I u_y^{(4)} \end{Bmatrix} + \begin{Bmatrix} \underline{f}_x \\ \underline{f}_y \end{Bmatrix} = \begin{Bmatrix} 0 \\ 0 \end{Bmatrix}, \tag{5.1}$$

in which u_x, u_y are the continuous displacements and $\underline{f}_x$, $\underline{f}_y$ are the external load components in the directions of the *x*- and *y*-axes, respectively. The Lagrange's notation was used to denote the derivatives with respect to *x*. The geometrical properties of the beam cross-section are the area $A=\tau t$ and the second moment of area $I=\tau t^3/12$. The cell wall elastic modulus E_s is the constant valued material property. The *x*-axis of the *xy*-coordinate system was assumed to coincide with the beam neutral axis.

Solutions to Eq. (5.1) for the cell walls were connected by the continuity conditions in terms of the displacements and rotations at the vertices and the equilibrium equations of the vertex points. In addition to this, the external load components were taken into consideration in the equilibrium equations of the vertices at the boundary domain $\partial\Omega$ [Publications III and IV].

5.2 Experimental design and setup

In accordance with the physical experiments on Nomex honeycombs, the simulation experiments on the effective in-plane stiffness were also conducted under a uni-axial tensile loading and simply supported boundary conditions in the laboratory *XY*-coordinate system as depicted in Fig. 5.2. More precisely, the boundary conditions were imposed in the way that the point 1 of the upper boundary extreme was pinned. The rest of the extreme followed the motion of the point 1 with the given rigid body constraint imposed by the fixture plates. Therefore, only the rotation around the *XY*-plane normal vector at point 1 was allowed for the upper boundary extreme. At the lower boundary extreme, the fixture plates imposed the rigid body constraint so that the rotation around the *XY*-plane normal vector at point 2 and the translation along *Y*-axis were allowed.

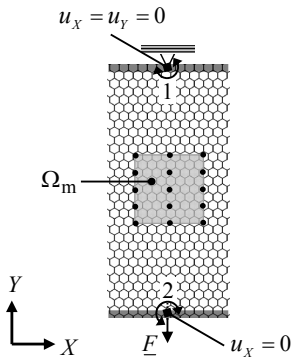

Figure 5.2: Schematic representation of the simulation experiment setup related to the effective in-plane stiffness: specimen, loading conditions and measurement domain Ω_m formed with the selected vertex points.

During these simulation experiments, displacement field was measured as a function of load $\underline{F}$, the computations of which were solely performed inside the measurement domain Ω_m presented in Fig. 5.2.

5.3 Results and discussions

5.3.1 Model validation

Physical experiments on the Nomex honeycombs were simulated so as to validate the proposed model. The same geometrical and mechanical properties and material orientation angles $\varphi \in \{0°, 45°, -45°, 90°\}$ as in the physical experiments were used.

Specimens of each sample designated with S-c-$\mathcal{T}$ were reconstructed for the use of simulation experiments by means of the variation terms for cell wall height and thickness α and β. These variation terms were determined through the measurements on the physically tested specimens. 80 specimens, i.e. 20 specimens for each φ, were tested to describe the effective in-plane stiffness properties of each sample S-*c*-$\mathcal{T}$ listed in Table 5.1 [Publication III].

Table 5.1: The effective stiffness properties obtained through the physical and simulation experiments on the Nomex honeycomb samples. Prefix Vi- stands for the determined values through the simulation model as provided in Publication III.

Sample	t/h	θ (°)	α	β	E_W (kPa)	E_L (kPa)	G_{WL} (kPa)	ν_{WL}	ν_{LW}	$-\eta_{WL,W}$	$-\eta_{WL,L}$
S-5-7	0.02	32	0.06	0.06	121.0	158.5	92.6	1.12	1.47	0.019	-0.103
Vi-S-5-7					113.9	152.2	87.3	1.01	1.35	0.076	-0.023
S-5-12	0.02	34	0.04	0.09	105.8	159.8	98.3	0.97	1.47	-0.049	0.004
Vi-S-5-12					119.3	148.3	94.6	0.98	1.22	0.018	0.115
S-6-7	0.0188	26	0.03	0.04	171.9	118.0	64.3	1.31	0.89	-0.048	0.077
Vi-S-6-7					161.2	113.9	58.1	1.23	0.87	-0.061	-0.056
S-6-12	0.0188	28	0.03	0.03	150.0	105.7	71.4	1.29	0.91	-0.104	-0.075
Vi-S-6-12					141.6	116.4	66.9	1.17	0.96	0.022	-0.081
S-13-7	0.0197	32	0.03	0.01	122.9	154.2	91.9	1.26	1.58	0.073	-0.069
Vi-S-13-7					126.0	150.2	80.3	1.08	1.28	-0.056	-0.059
S-13-12	0.0191	32	0.03	0.01	96.5	128.2	84.6	0.91	1.21	0.004	0.024
Vi-S-13-12					114.9	136.8	76.6	0.94	1.13	-0.044	0.038

Table 5.1 indicates that similar results were obtained in both the physical and simulation experiments. However, the maximum relative error between the physical and simulation experiments was 19.0% for E_W of the sample S-13-12, while the minimum relative error was 1.1% for ν_{WL} of the sample S-5-12. The relative error was possibly originated from the boundary artifacts and the measurement errors in the physical experiments and the modeling errors in the simulation experiments. The boundary artifacts can be due to eccentric loads and constrained rotational degree of freedom because of the friction at the contact surface of the fixture plates and actuator. The measurement errors can be due to the resolution of in-situ digital images and signal processing problems in controllers and transducers, whereas the modeling errors can be related to the selection of deformation mechanisms and geometric input data.

5.3.2 Effects of the cell wall height and thickness variations

After validating the model, the simulation experiments were conducted to understand the effects of the variations related to the cell wall height and thickness on the effective in-plane stiffness. For this case, 16 samples were specified in terms of $\alpha \in \{0, 0.05, 0.10, 0.15\}$ and $\beta \in \{0, 0.05, 0.10, 0.15\}$ where the number of specimens in each sample was 20. The values of α and β were chosen in accordance with the measured values in Table 5.1. The geometrical properties were c=10 mm, τ=7 mm, θ=30°, the cell wall

thickness-to-height ratio t/h=0.023 and E_s=7.9 GPa as reported in Publication III.

The simulation experiment results in Fig. 5.3 indicate that the cell wall thickness variations had an impact on the effective in-plane elastic moduli E_W, E_L, and the shear modulus G_{WL}. This can be related to the increase in the number of the thicker cell walls that counteracted the effect of the slender ones. The influence of cell wall thickness variations on the effective Poisson's ratios ν_{WL}, ν_{LW} was found to be weak.

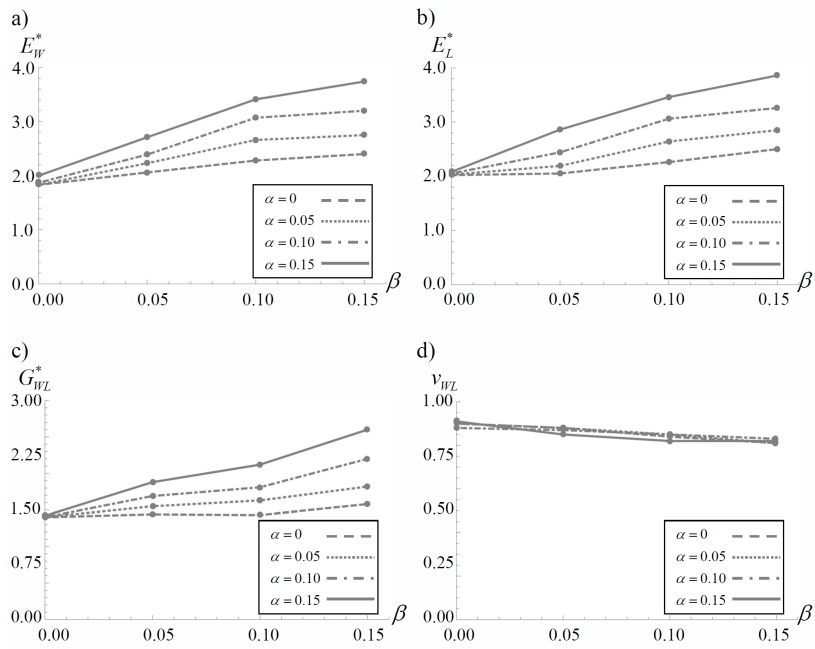

Figure 5.3: Effect of the cell wall thickness variations on the non-dimensional effective in-plane elastic properties. $E_W^* = E_W/\underline{E}$, $E_L^* = E_L/\underline{E}$, $G_{WL}^* = G_{WL}/\underline{E}$, in which $\underline{E} = E_s(t/h)^3$. Linear interpolation is used to connect the consecutive data points [Publication III].

Similarly, the simulation experiment results in Fig. 5.4 indicate that the cell wall height variations had an effect on E_W, E_L, and G_{WL}; however, the influence on ν_{WL}, ν_{LW} was insignificant. One of the reasons for this effect on the effective in-plane elastic and shear moduli can be due to the likely cell shape and topology changes with increasing α, which can lead to transitions in deformation mechanisms, e.g. from cell wall bending to cell wall stretching [Li et al., 2006; Alkhader and Vural, 2008; Deshpande et al., 2001; Wang et al., 2005]. This outcome was more evident for higher β as seen in Fig. 5.4.

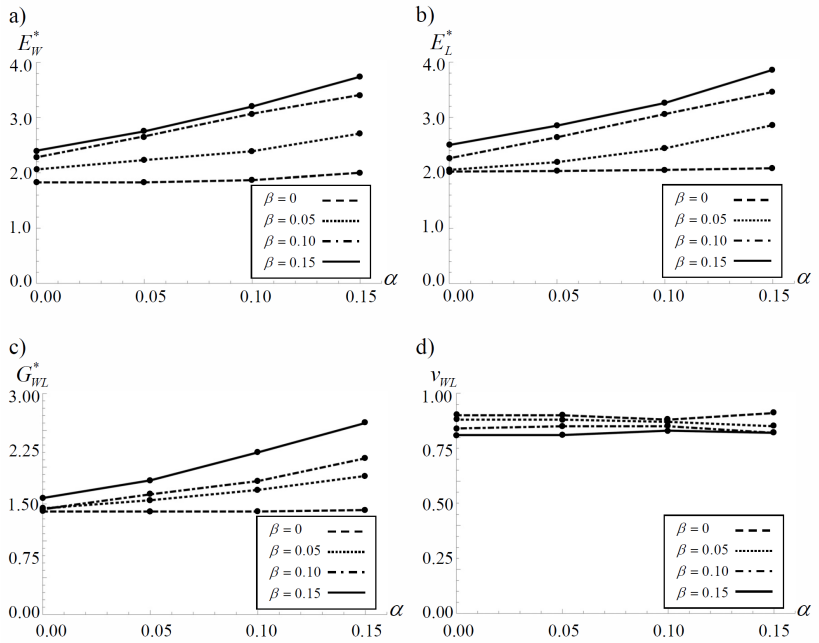

Figure 5.4: Effect of the cell wall height variations on the non-dimensional effective in-plane elastic properties. $E_W^* = E_W / \underline{E}$, $E_L^* = E_L / \underline{E}$, $G_{WL}^* = G_{WL} / \underline{E}$, in which $\underline{E} = E_s (t/h)^3$. Linear interpolation is used to connect the consecutive data points [Publication III].

6. Overview of the strength assessments

6.1 Cellular material strength

In the present study, cellular material strength was defined as the threshold at which the first failing cell wall was detected in a cellular material subjected to external stress **s**. Based on this definition, it was possible to associate the cellular material strength with the microscopic failure mechanisms, e.g. cell wall bending and stretching, which can cause cell wall breaking, peeling, etc., as illustrated in Fig. 6.1.

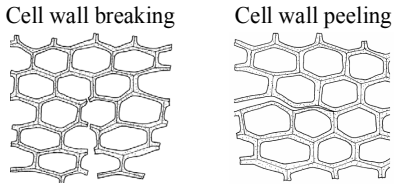

Figure 6.1: Schematic representation of cell wall breaking and peeling in a softwood species as a result of microscopic failure mechanisms [Ashby et al., 1985].

The cellular material strength was quantified in terms of the failure mechanisms and corresponding failure criteria. For instance, if a cellular material is composed of n cell walls and stress resultants, e.g. bending moment M and normal force N, on a cell wall are considered, the failure criteria for the j^{th} cell wall can be defined as $g_j^1 = \left|M_j\right| / M_{\text{cr}}$ and $g_j^2 = \left|N_j\right| / N_{\text{cr}}$. In these criteria, $|M_j|$ and $|N_j|$ are the absolute values of the bending moment and normal force for the j^{th} cell wall whilst M_{cr} and N_{cr} are the critical values as the material properties. The failure criteria $g_j^i \le 1$ for $i \in \{1, 2\}$ and $j \in \{1, 2, \ldots, n\}$ restrict the magnitude of the stress resultants and the j^{th} cell wall fails whenever $g_j^i = 1$. Assuming that the stress resultants depend linearly on the external stress **s**, one may obtain the

cellular material strength in terms of the critical stress [Karakoç and Freund, 2012; Karakoç and Freund, 2013]

$$\mathbf{s}_{\mathrm{cr}} \equiv p\underline{\mathbf{s}} = \min_{i\in\{1,2,\ldots,m\}} \frac{1}{\max_{j\in\{1,2,\ldots,n\}} g_j^i}\underline{\mathbf{s}} \tag{6.1}$$

for $i \in \{1, 2,\ldots, m\}$ failure mechanisms and $j \in \{1, 2,\ldots, n\}$ cell walls. Here, $p \in \mathbb{R}^+$ is the linear scaling term and used to detect the first failing cell wall.

In accordance with Eq. (6.1), the present strength assessment aimed to (1) identify the linear scaling term(s) p associated with the assumed failure mechanisms and the corresponding failure criteria and (2) to determine the cellular material strength in relation to the safe region in stress space and its depence on the geometrical properties.

6.2 Strength assessment methods

In the present study, the strength was taken to be a statistical quantity depending on the variation term for cell wall height α and the scale $V=(\mathcal{W}/h^{\circ})(\mathcal{L}/h^{\circ})$ comprehended from Fig. 5.1. Hence, the strength assessment was performed by employing statistical tools, which are briefly explained below.

6.2.1 A statistical description for strength through cumulative distribution functions

In the statistical theory, strength can be described with its probability density function or more conveniently with the cumulative distribution function. The latter gives the probability with which a specimen fails under the critical stress $\mathbf{s}_{\mathrm{cr}}$.

In the present strength assessment, specimens were generated for each sample specified with α and V. Then, simulation experiments were conducted and $\mathbf{s}_{\mathrm{cr}}$ was obtained for each specimen by means of the defined failure criterion based on cell wall bending $g_j^1 = |M_j| / M_{\mathrm{cr}}$ for $j \in \{1, 2,\ldots, n\}$ cell walls. The $\mathbf{s}_{\mathrm{cr}}$ values were used to describe the in-plane strength characteristics of each sample in the direction of $\underline{\mathbf{s}}$ in the stress space illustrated in Fig. 6.2.

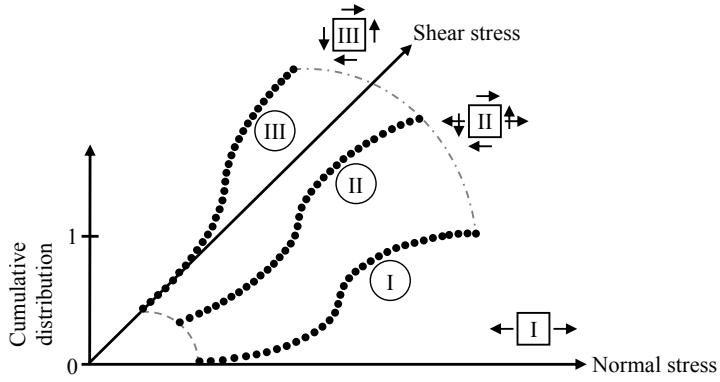

Figure 6.2: Illustration of cumulative distribution function plots used to describe the in-plane strength characteristics of a sample in the direction of external stress $\underline{\mathbf{s}}$ in normal-shear stress space. Black dots represent the critical stress $\mathbf{s}_{cr}$ value determined for each specimen. Dashed and dashed-dotted lines show the minima and maxima of the cumulative distributions [Publication IV].

For non-dimensional strength analysis, linear scaling term p of Eq. (6.1) was used instead of the critical stress $\mathbf{s}_{cr}$. The p values for a sample were represented as set elements; thus, $P=\{p_1, p_2,..., p_n\}$, for which n is the number of tested specimens in the sample. For comparison purposes, these sets were normalized by means of the constant scaling term p^o of regular cellular material with $\alpha=0$ depicted in Fig. 5.1. The normalized scaling term set for a sample was represented as $\Pi=\{p_1/p^o, p_2/p^o,..., p_n/p^o\}$. Then, the cumulative distribution function for a sample in the direction of $\underline{\mathbf{s}}$ in the stress space was expressed as

$$\mathrm{cdf}(p/p^o,\alpha,V)=\frac{\left|\{p/p^o\in\Pi : p_j/p^o\le p/p^o\}\right|}{|\Pi|} \tag{6.2}$$

for $j\in\{1, 2,..., n\}$ specimens. Here, $|\ |$ denotes the set size. The cumulative distribution function of Eq. (6.2) describes the strength statistics in terms of the failure initiation. Alternatively, one may think that Eq. (6.2) gives an estimate for the proportion of the sample failing before p/p^o.

The cumulative distribution data obtained from Eq. (6.2) was fitted and parameterized with the three parameter Weibull distribution [Weibull, 1939]. Thus,

$$\mathrm{cdf}(p/p^o,\alpha,V)=1-\exp\left(-\left(\frac{p/p^o-\Pi_{\min}}{\lambda}\right)^{\kappa}\right), \tag{6.3}$$

in which λ and κ are the scale and shape parameters, and $\Pi_{\min}$ is the minimum value obtained from the set Π of the corresponding sample.

6.2.2 Scale effect on the strength statistics

In the present strength assessment based on the failure initiation, the specimen was assumed to be composed of constituents in series system. Therefore, the constituents were assumed to survive or fail independently of one another [Sutherland et al., 1999; Weibull, 1939]. Hence, under an external stress $\underline{\mathbf{s}}$, the failure initiation probability of the specimen cdf($\underline{\mathbf{s}}$) was related to the failure probability of the constituent $\mathrm{cdf}_i(\underline{\mathbf{s}})$. Assuming identical failure probabilities for all the constituents, this relationship is expressed as [Danielsson, 2009; Suo et al., 2012]

$$\mathrm{cdf}(\underline{\mathbf{s}}) = 1 - \left(1 - \mathrm{cdf}_i(\underline{\mathbf{s}})\right)^n . \tag{6.4}$$

In Eq. (6.4), n is the number of constituents and taken to be equal to the scale ratio between the specimen and the constituents, i.e. $n=V/\Delta V$. Similarly, in case of strength analysis for two different samples formed with specimens of similar constituents but different scales V_1 and V_2, n can be used as a linking term, i.e. $n=V_2/V_1$. By knowing the strength (failure initiation) statistics of the sample with V_1, the strength statistics of the other sample can be obtained through [Suhaimi and Saleh, 2005; Tabiei and Sun, 2000]

$$\mathrm{cdf}(\underline{\mathbf{s}}, V_2) = 1 - \left(1 - \mathrm{cdf}(\underline{\mathbf{s}}, V_1)\right)^{V_2/V_1} . \tag{6.5}$$

Similar to Eq. (6.5), the cumulative distribution functions of the samples with different V_1 and V_2 but the same α in the direction of $\underline{\mathbf{s}}$ was related to each other. In accordance with Eq. (6.2), this relationship was expressed as

$$\mathrm{cdf}(p/p^0, \alpha, V_2) = 1 - \left(1 - \mathrm{cdf}(p/p^0, \alpha, V_1)\right)^{V_2/V_1} . \tag{6.6}$$

7. Simulation experiments on the strength properties

7.1 General remarks

The introduced micromechanical model in Publication III was further developed in Publication IV so as to (1) determine the critical stress values $\mathbf{s}_{cr}$ at the failure initiation describing the cellular material strength in the transverse plane and (2) to analyze the effects of cell wall height variations and scale on the strength in a statistical manner. Eventually, a statistical strength (failure initiation) model was proposed to estimate the cellular material strength in the normal-shear stress space.

7.2 Experimental design and setup

The variation term for cell wall height α and the scale $V=(\mathcal{W}/h^o)(\mathcal{L}/h^o)$ (assuming equal values for $\mathcal{W}$ and $\mathcal{L}$) were used to generate the specimens for the simulation experiments on the cellular material strength. 500 specimens were formed for each sample specified with $\alpha \in \{0, 0.03, 0.15, 0.20, 0.30\}$ and $V \in \{100, 400, 1600, 3600\}$. Cell wall thickness t was taken to be constant so that the related variation term β=0. The α values were chosen to avoid possible geometrical problems such as cell wall overlapping as illustrated in Fig. 7.1.

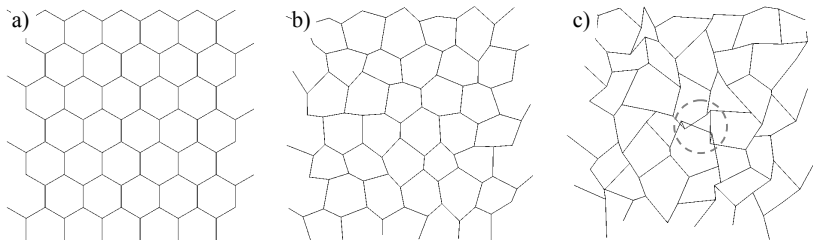

Figure 7.1: Geometries of increasing cell wall height variations: a) α=0, b) α=0.30, c) α=0.60 (not covered in the present study). Circle with dashed line shows a cell wall overlapping location.

Three different external stress $\underline{\mathbf{s}}$ were applied to the specimens through the cell wall ends (vertices) on the boundary domain $\partial\Omega$ depicted in Fig. 7.2: (1) uniaxial tension, i.e. $\underline{s}_{XX}=s$, $\underline{s}_{XY}=\underline{s}_{YX}=\underline{s}_{YY}=0$, (2) combined loading, i.e. $\underline{s}_{XX}=\underline{s}_{XY}=\underline{s}_{YX}=s$, $\underline{s}_{YY}=0$, (3) pure shear, i.e. $\underline{s}_{XY}=\underline{s}_{YX}=s$, $\underline{s}_{XX}=\underline{s}_{YY}=0$. Measurement domain Ω_m was taken to be smaller than the entire solution domain in order to reduce the effects of likely artifacts caused by $\underline{\mathbf{s}}$.

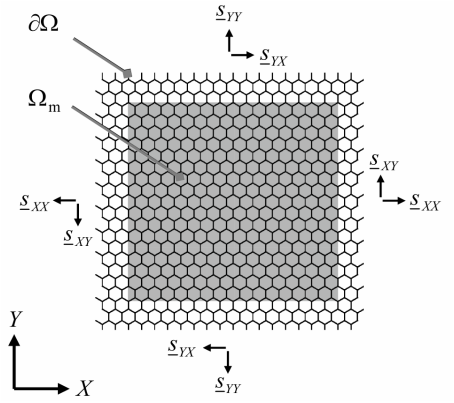

Figure 7.2: Schematic representation of the specimen and the simulation experiment setup related to the strength: external stress $\underline{\mathbf{s}}$, or explicitly $\underline{s}_{ij}$ for $i, j \in \{X, Y\}$, the boundary domain $\partial\Omega$ and the measurement domain Ω_m.

The critical stress value $\mathbf{s}_{cr}$, or explicitly s_{ij} for $i, j \in \{X, Y\}$, resulting in the first failing cell wall was separately determined for each specimen. Cell wall bending was taken to be the decisive failure mechanism and cell walls started to fail whenever the maximum magnitude of the bending moments exceeded the critical bending moment M_{cr}. Therefore,

$$\mathbf{s}_{cr} \equiv p\,\underline{\mathbf{s}} = \frac{M_{cr}}{\max_{j\in\{1,2,\ldots,n\}}\left|M_j\right|}\underline{\mathbf{s}}. \tag{7.1}$$

In this expression, p is the linear scaling term and M_j is the bending moment taken over $j \in \{1, 2, \ldots, n\}$ cell walls inside the measurement domain Ω_m presented in Fig. 7.2.

7.3 Results and discussions

The simulation experiment results were explained in detail for the specimens tested under uniaxial tension. The results related to combined loading and pure shear were briefly discussed.

7.3.1 Effects of the cell wall height variations and the scale

The present simulation experiments show that the strength of regular cellular materials, for which α=0, was a deterministic quantity and did not depend on the scale V. The outcome was the normalized scaling term set Π={1, 1,.., 1} that was defined with $\Pi_j = p_j / p^o$ for $j \in \{1, 2, ..., n\}$ specimens in the direction of $\underline{\mathbf{s}}$, in which p^o is the constant scaling term for a regular cellular material. Thus, the global maximum normalized scaling value $\Pi_{\max}^{\text{glob}}$ was equal to unity.

On the other hand, non-deterministic behavior was observed with the increasing cell wall height variations, e.g. the location of the first failing cell wall in Fig. 7.3. This can be explained so that once the variation term α increases, there occurs to be distortions in the alignments of the cell walls with respect to the loading direction. Under the circumstances, there was uneven distribution of the bending moments on the cell wall ends. Hence, it was likely for each tested specimen to have different strength and first failing cell wall location. In addition to this, higher bending moments were obtained than those of the (more) regular materials resulting in lower cellular material strength in accordance with Eq. (7.1). This can also be seen from the cumulative distribution function plots in Fig. 7.4 [Publication IV].

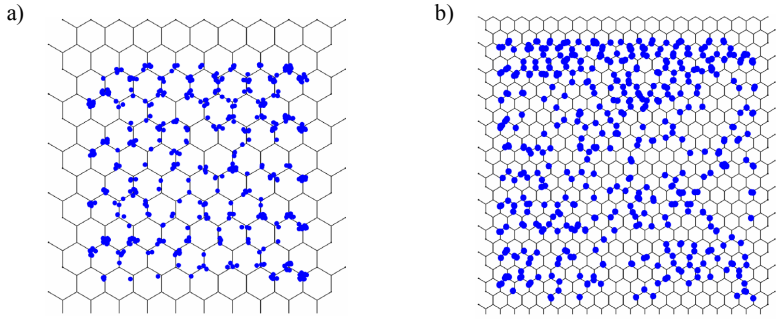

Figure 7.3: Locations of the first failing cell walls. Samples with: a) α=0.30 and V=100, b) α=0.30 and V=400. In order to describe the strength properties of each sample, 500 specimens were tested.

The cumulative distribution function plots of Fig. 7.4 show that the strength decreased with increasing scale V. In other words, the failure initiation probability became higher for larger cellular materials compared to the smaller ones under the same $\underline{\mathbf{s}}$. In case of analyzing the sample with extremely large V=40000, this probability was assumed to reach the global minimum normalized scaling value $\Pi_{\min}^{\text{glob}}$, which was obtained in the

direction of **s** with the proposed extrapolation method [for details, see Publication IV].

In addition to the separate effects of α and V, the cumulative distribution function plots of Fig. 7.4 also show that increase in both α and V resulted in lower cellular material strength.

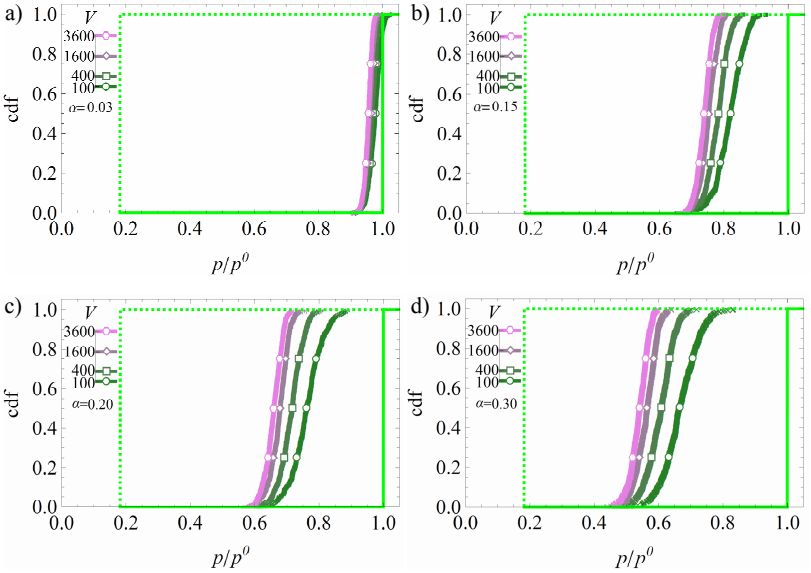

Figure 7.4: Cumulative distribution function plots for the failure initiation of the cellular material samples under uniaxial tension, $\underline{s}_{XX}=s$, $\underline{s}_{XY}=\underline{s}_{YX}=\underline{s}_{YY}=0$: a) α=0.03, b) α=0.15, c) α=0.20, d) α=0.30. The dashed and solid straight lines represent the cumulative distributions for the samples with V=40000 (extremely large scale) and α=0 (regular cellular geometry), respectively. The vertical dashed and solid lines represent the global minimum and maximum values $\Pi_{\min}^{\text{glob}}$, $\Pi_{\max}^{\text{glob}}$.

7.3.2 Statistical strength (failure initiation) model

The effects of α and V on the strength was modeled by further processing the cumulative distribution data. Cumulative distribution data of a reference sample with α_{ref} and V_{ref} in the direction of **s** were first fitted to the three parameter Weibull distribution. Then, the distribution was inserted into the statistical relation of Eq. (6.6) to estimate the strength (failure initiation) statistics of the target samples with different V but same α_{ref} in the direction of **s**.

As an example, reference samples with α_{ref}=0.15 and V_{ref}=400, and α_{ref}=0.30 and V_{ref}=400 under the uniaxial tension were considered. The computations were carried out for the target samples specified with

$V \in \{100, 1600, 3600\}$ and the estimated distribution functions were plotted in Fig. 7.5. It was deduced that the estimations were accurate and in good agreement with the cumulative distribution functions of the target samples. However, the estimations of this model were limited to the α_{ref} value.

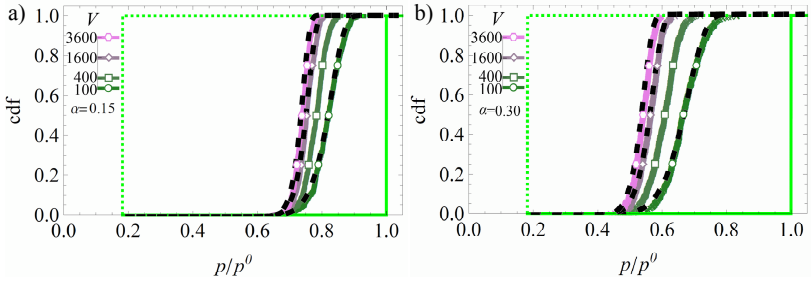

Figure 7.5: Estimated cumulative distribution function plots based on the reference samples under the uniaxial tension and specified with: a) α_{ref}=0.15 and V_{ref}=400, b) α_{ref}=0.30 and V_{ref}=400. Black dashed lines represent the estimated distribution functions, while the solid lines represent the reference sample data.

In order to overcome this limitation and to form a generic model, it was necessary to express the scale parameter λ and the shape parameter κ of the Weibull distribution as functions of α instead of constant terms. This provided a basis to estimate the failure initiation statistics of the samples with different α and V values in the direction of $\underline{\mathbf{s}}$ by just knowing the statistics of the reference samples. This model was expressed as [Publication IV]

$$\text{cdf}(p/p^{\text{o}}, \alpha, V) = 1 - \exp\left(-\left(\frac{p/p^{\text{o}} - \Pi_{\text{min}}^{\text{glob}}}{\lambda(\alpha)} \right)^{\kappa(\alpha)} \right)^{V/V_{\text{ref}}}, \qquad (7.2)$$

in which $\lambda(\alpha)$ and $\kappa(\alpha)$ are the interpolation functions. These functions were determined through the discrete values of λ and κ for the samples with a selected reference scale V_{ref} and different values of α.

The proposed model in Eq. (7.2) was studied by using the reference samples designated with $\alpha \in \{0.03, 0.15, 0.20, 0.30\}$ and V_{ref}=400. The cumulative distribution data of these samples were fitted by using the three parameter Weibull distribution. Calculated values of the parameters λ and κ, and $\Pi_{\text{min}}^{\text{glob}}$ are listed in Table 7.1 for the investigated conditions, i.e. uniaxial tension, combined loading and pure shear.

Table 7.1: Weibull parameters λ and κ, and $\Pi_{\min}^{glob}$ fitted for the cumulative distribution functions of the samples with different irregularities α but same V_{ref}=400. Tested loading conditions were (1) the uniaxial tension, (2) the combined loading, (3) the pure shear.

α	Uniaxial tension		Combined loading		Pure shear	
	λ	κ	λ	κ	λ	κ
0.03	0.76	60.21	0.75	71.7	0.79	102.2
0.15	0.58	20.67	0.54	21.6	0.61	24.2
0.20	0.52	16.31	0.48	18.1	0.55	19.9
0.30	0.41	10.91	0.39	12.7	0.48	14.2
$\Pi_{\min}^{glob}$	0.17		0.18		0.17	

As a result of this process, the statistical strength (failure initiation) model was formed for the corresponding loading conditions. This model was represented in the normal-shear stress space by replacing p/p^o of Eq. (7.2) with $p=\mathbf{s}_{cr}/\underline{\mathbf{s}}$ of Eq. (7.1), in which the constant scaling term p^o=2.64 for the uniaxial tension, p^o=1.29 for the combined loading and p^o=1.32 for the pure shear conditions [Publication IV]. The graphical representation of the model for the tested loading conditions is given in Fig. 7.6. The figure presents the estimated strength percentiles for the sample specified with α=0.30 and V=2500 in the normal-shear stress space by means of the proposed model in Eq. (7.2). Hence, percentage of failing specimens under a loading condition and the corresponding stress values can be readily estimated.

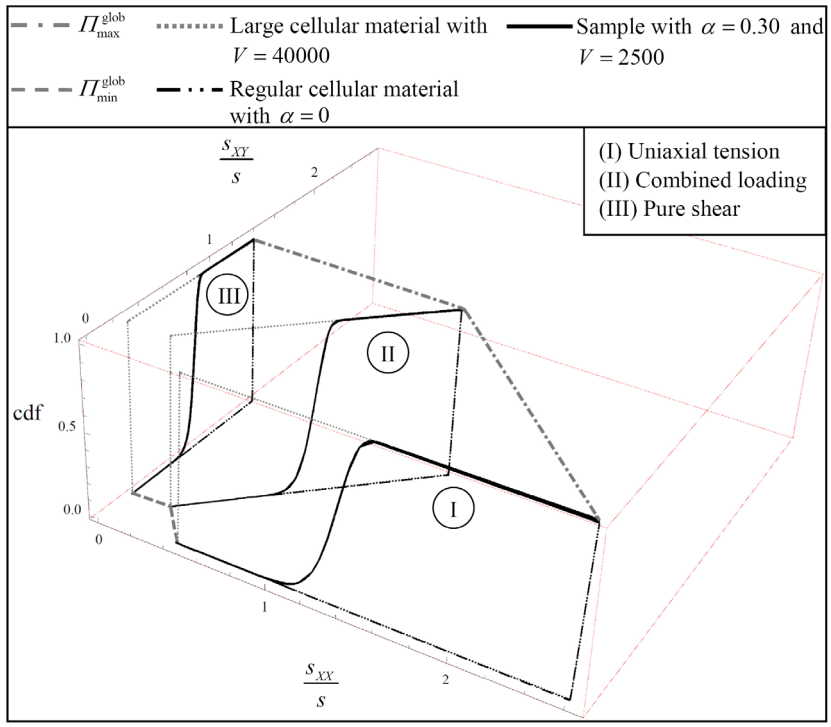

Figure 7.6: Estimated cumulative distribution function plots in the normal-shear stress space obtained through the proposed model.

8. Conclusions

8.1 Summary and conclusions

The present study was conducted to investigate the effective stiffness and strength properties of the cellular materials in the transverse plane and their dependence on the cellular structure. For this purpose, two novel approaches comprising (1) an experimental method for determining the effective in-plane stiffness properties and (2) a statistical simulation model for describing the effects of the scale and the variations related to the cell geometry on the effective in-plane stiffness and strength properties were proposed.

The introduced experimental method was used in the measurements on two different cellular materials which were the Nomex honeycombs and the Norway spruce. As a result of these experiments, effective in-plane elastic moduli, Poisson's ratios, shear modulus and coefficients of mutual influence characterizing the coupling between the shearing and normal stresses were determined.

In order to obtain the effective in-plane stiffness properties, uni-axial experiment setups were introduced, for which the effects of boundary artifacts were reduced. The measurement errors in the displacement field data were minimized with the proposed image processing techniques, the marker tracking technique for the honeycomb specimens and the digital image correlation for the wood specimens, in replacement of the conventional equipments such as linear variable differential transformer LVDT. Cellular materials were tested for different material orientations, $\varphi \in \{0°, 45°, -45°, 90°\}$ for Nomex honeycombs and $\varphi \in \{0°, 15°, 30°, 45°, 60°, 75°, 90°\}$ for Norway spruce. Thereafter, stress and strain field data obtained from the experiments were processed with the proposed analysis method based on the transformation rule and the least squares function. Hence, the effective stiffness properties of the investigated cellular materials in the transverse plane were obtained as the unique minimizer.

The analyses show that the tested cellular materials can be classified as orthotropic in the plane of interest and the investigated material coordinate systems can serve as the principal material coordinate systems.

The current statistical simulation model was designed to represent the heterogeneous nature of the cellular materials by using beam networks. The model was first validated through the comparison with the physical experiments on the effective stiffness properties of Nomex honeycombs in the transverse plane. The model estimated the effective in-plane stiffness properties within the relative error range of 1.1%-19%. The outcome was promising for the modeling aspect when compared to the investigated analytical model resulting in a relative error range of 0.5%-28.0%.

Following the model validation, the simulation experiments were carried out to study the effects of the geometrical properties on the effective in-plane stiffness properties of cellular materials. The results of both the physical and simulation experiments on the effective in-plane stiffness show that the stiffness properties were highly affected by the geometrical characteristics of the cellular structure. Changes in the corner angles and cell wall thickness-to-height ratio, cell wall height and thickness variations were observed to have influences on the effective in-plane elastic and shear moduli. Therefore, these parameters should be carefully considered in designing and modeling cellular materials.

The proposed model was further developed. Simulation experiments were conducted and a statistical strength (failure initiation) model was presented. The strength in this context was defined to be the stress resulting in the first failing cell wall in the cellular material. A failure criterion was introduced and studied by using cell wall bending as the failure mechanism. The simulation experiment results were analyzed by using cumulative distribution functions and parameterized with the three parameter Weibull distribution to study the effects of cell wall height variations and scale. The analyses reveal that the failure initiation was more likely for the samples with increasing scale. Similarly, the increasing cell wall height variations affected the cellular material strength.

8.2 Future developments

In the present study, the effective stiffness properties were determined by using the transformation rule and the least squares function in both the physical and simulation experiments. Therefore, the compliance matrix

components were determined as the unique minimizer of the least squares function. However, the analysis method can be improved to find the variance of the compliance for each sample, e.g. by random sampling of the stress-strain data determined for each different material orientation of the studied sample.

The physical and simulation experiments and the proposed methods in this study can be further improved in many ways. The present study only deals with the determination of the effective stiffness and strength properties of the cellular materials in the transverse plane. A more comprehensive model can be thus developed to determine the mechanical properties in three dimensional space by taking other possible deformation and failure mechanisms such as buckling and debonding into consideration. In addition to this, possible extensions for the environmental effects, e.g. temperature and moisture, on the mechanical properties can also be implemented to advance the current state of the art in cellular material modeling.

References

Aboudi J (1995). Micromechanical analysis of thermoinelastic multiphase short-fiber composites. Composites Engineering; 5(7): 839-850.

Alkhader M, Vural M (2008). Mechanical response of cellular solids: Role of cellular topology and microstructural irregularity. International Journal of Engineering Science; 46(10): 1035-1051.

Andrews EW, Gibson LJ, Ashby MF (1999). The creep of cellular solids. Acta Metallurgica; 47(10): 2853-2863.

Angst-Nicollier V (2012). Moisture induced stresses in glulam: Effect of cross section geometry and screw reinforcement. Doctoral dissertation, Trondheim, Norwegian University of Science and Technology.

Ashby MF, Easterling KE, Harrysson R, Maiti SK (1985). The fracture and toughness of woods. Proceedings of the Royal Society of London.A. Mathematical and Physical Sciences; 398(1815): 261-280.

Balawi S, Abot JL (2008). A refined model for the effective in-plane elastic moduli of hexagonal honeycombs. Composite Structures; 84(2): 147-158.

Bitzer T (1997). Honeycomb technology: materials, design, manufacturing, apllications and testing. Glasgow: Chapman & Hall.

Bramwell D (1976). Flora of Canary islands: Pocket guide. Editorial Rueda.

Brändström J (2001). Micro- and ultrastructural aspects of Norway spruce tracheids: A review. International Association of Wood Anatomists IAWA Journal ;22 (4): 333–353.

Carrington H (1923). The elastic constants of spruce. Philosophical Magazine; 45: 1055-1057.

Chen C, Lu TJ, Fleck NA (1999). Effect of imperfections on the yielding of two-dimensional foams. Journal of the Mechanics and Physics of Solids; 47(11): 2235-2272.

Chen C, Fleck NA (2002). Size effects in the constrained deformation of metallic foams. Journal of the Mechanics and Physics of Solids; 50(5): 955-977.

Chen DH, Horii H, Ozaki S (2009). Analysis of in-plane elastic modulus for a hexagonal honeycomb core: Analysis of Young's modulus and shear modulus. Journal of Computational Science and Technology; 3(1): 1-12.

Dahl KB (2009). Mechanical properties of clear wood from Norway spruce. Doctoral dissertation, Trondheim, Norwegian University of Science and Technology.

Dahl KB, Malo KA (2009). Linear shear properties of spruce softwood. Wood Science and Technology; 43(5-6): 499-525.

Danielsson H (2009). The strength of glulam beams with holes: A Probabilistic Fracture Mechanics Method and Experimental Tests. Licentiate dissertation, Lund, Lund University.

Deshpande VS, Ashby MF, Fleck NA (2001). Foam topology: bending versus stretching dominated architectures. Acta Materialia; 49(6): 1035-1040.

Dill-Langer G, Lütze S, Aicher S (2002). Microfracture in wood monitored by confocal laser scanning microscopy. Wood Science and Technology; 36(6): 487-499.

DuPont-Nomexpaper type 410 technical data sheet (2013). (Available online: http://www2.dupont.com/Energy_Solutions/en_US/products/paper (Last check: Sept 2013)).

DuPont-Nomexfiber technical guide (2013). (Available online: http://www.nakedwhiz.com/gasketsafety/nomextechnicalguide.pdf (Last check: Sept 2013)).

Evans AG, Hutchinson JW, Ashby MF (1999). Multifunctionalityf of cellular metal systems. Progress in Materials Science; 43: 171-221.

Farruggia F, Perré P (2000). Microscopic tensile tests in the transverse plane of earlywood and latewood parts of spruce. Wood Science and Technology; 34(2): 65-82.

Garab J, Keunecke D, Hering S, Szalai J, Niemz P (2010). Measurement of standard and off-axis elastic moduli and Poisson's ratios of spruce and yew wood in the transverse plane. Wood Science and Technology; 44(3): 451-464.

Gibson LJ, Ashby MF, Schajer GS, Robertson CI (1982). The mechanics of two dimensional cellular materials. Proceedings of the Royal Society of London.A.Mathematical and Physical Sciences; 382(1782): 25-42.

Gibson LJ, Ashby MF (1999). Cellular solids: structure and properties. Cambridge: Cambridge University Press.

Gustafsson PJ (2003). Fracture perpendicular to grain-structural applications. In: Timber engineering edited by Thelandersson S, Larsen HJ. Chichester: John Wiley and Sons: 103-130.

Hassel BI, Berard P, Modén CS, Berglund LA (2009). The single cube apparatus for shear testing–Full-field strain data and finite element analysis of wood in transverse shear. Composites Science and Technology; 69(7–8): 877-882.

Havimo M, Rikala J, Sirviö J, Sipi M (2008). Distributions of tracheid cross-sectional dimensions in different parts of Norway spruce stems. Silva Fennica; 42(1): 89–99.

Herrmann HJ, Roux S (1990). Statistical models for the fracture of disordered media (Random Materials and Processes). Amsterdam: North-Holland.

Hexcel product data sheet (2013). (Available online: http://www.hexcel.com/resources/honeycomb-data-sheets (Last check: Sept 2013)).

Holmberg S, Persson K, Petersson H (1999). Nonlinear mechanical behaviour and analysis of wood and fibre materials. Computers and Structures; 72(4–5): 459-480.

Hou B (2011). Dynamic enhancement and multi-axial behavior of honeycombs under combined shear-compression. Doctoral dissertation, Paris, Ecole Normale Supérieure de Cachan.

Jernkvist L, Thuvander F (2001). Experimental determination of stiffness variation across growth rings in Picea abies. Holzforschung; 55(3): 309-317.

Jones R (1975). Mechanics of composite materials. Washington, D.C.: McGraw-Hill Book Company.

Kahle E, Woodhouse J (1994). The influence of cell geometry on elasticity of softwood. Journal of Materials Science; 29(5): 1250-1259.

Karakoç A, Freund J (2012). A statistical representation of failure for cellular materials. Proceedings of European Congress on Computational Methods in Applied Sciences and Engineering, Vienna, September 10-14.

Karakoç A, Freund J (2013). Statistical strength analysis for honeycomb materials. International Journal of Applied Mechanics; 5(2): 1350021 (12).

Kaw A (2006). Mechanics of composite materials, vol. 2nd Ed. Boca Raton: Taylor-Francis Group.

Kollmann F, Côté W (1968). Principles of Wood Science and Technology - Solid Wood, vol. 1st Ed. Berlin: Springer Verlag.

Kumar RS, McDowell DL (2004). Generalized continuum modeling of 2-D periodic cellular solids. International Journal of Solids and Structures; 41(26): 7399-7422.

Landis E, Vasic S, Davids WG, Parrod P (2002). Coupled experiments and simulations of micro-structural damage in wood. Experimental mechanics; 42(4): 389-394.
Lekhnitskii SG (1981) Theory of elasticity of an anisotropic body. Moscow: Mir Publishers.

Li K, Gao XL, Subhash G (2006). Effects of cell shape and strut cross-sectional area variations on the elastic properties of three-dimensional open-cell foams. Journal of the Mechanics and Physics of Solids; 54(4): 783-806.

Malvern LE (1969). Introduction to the mechanics of a continuous medium. New Jersey: Prentice Hall.

Marin JC, Canas J, Paris F, Morton J (2002). Determination of G12 by means of the off-axis tension test.: Part I: review of gripping systems and correction factors. Composites Part A: Applied Science and Manufacturing; 33(1): 87-100.

Mascia NT, Vanalli L (2012). Evaluation of the coefficients of mutual influence of wood through off-axis compression tests. Construction and Building Materials; 30: 522-528.

Masters I, Evans K (1996). Models for the elastic deformation of honeycombs. Composite Structures; 35(4): 403-422.

MIL-STD-401B (1967). Military standard sandwich constructions and core materials, general test methods. Washington D.C.: Department of Defense.

Modén CS (2008). Micromechanics of softwoods in the transverse plane - effects on cell and annual ring scales. Doctoral dissertation, Stockholm, KTH Royal Institute of Technology.

Nemat-Nasser S, Hori M (1999). Micromechanics: Overall properties of heterogeneous materials. Amsterdam: North Holland.

Parnes R (2001). Solid mechanics in engineering. Chichester: John Wiley & Sons.

Persson K (2000). Micromechanical modeling of wood and fibre properties. Doctoral dissertation, Lund, Lund University.

Petric B, Ščukanec V (1973). Volume percentage of tissues in wood of conifers grown in Yugoslavia. International Association of Wood Anatomists IAWA Bulletin; 2: 3–7.

Ren ZY, Zheng QS (2002). A quantitative study of minimum sizes of representative volume elements of cubic polycrystals-numerical experiments. Journal of Mechanics and Physics of Solids; 50(4): 881-893.

SCAN-test: Scandinavian pulp, paper and board testing committee (1993). Identification of machine and cross directions. Stockholm: ScanP9-93.

Schwingshackl CW, Aglietti GS, Cunningham PR (2006). Determination of honeycomb material properties: existing theories and an alternative dynamic approach. Journal of Aerospace Engineering; 19(3): 177-183.

Silva MJ, Gibson LJ (1997). The effects of non-periodic microstructure and defects on the compressive strength of two-dimensional cellular solids. International Journal of Mechanical Sciences; 39(5): 549-563.

STEP/EUROFORTECH (1995). Timber Engineering-STEP 1. Almere: Centrum Hout.

Suhaimi AB, Saleh AL (2005). Verification of Weibull's theory of brittle fracture to Meranti's timber loaded in tension parallel to the grain. Jurnal Teknologi; 43(B): 27-34.

Suo B, Cheng Y, Zeng C, Li J (2012). Calculation of failure probability of series and parallel systems for imprecise probability. International Journal of Engineering and Manufacturing; 2: 79-85.

Sutherland LS, Shenoi RA, Lewis SM (1999). Size and scale effects in composites: I. Literature review. Composites Science and Technology; 59(2): 209-220.

Tabiei A, Sun J (2000). Analytical simulation of strength size effect in composite materials. Composites Part B: Engineering; 31(2): 133-139.

Tuttle M (2003). Structural analysis of polymeric composite materials. New York: Marcel Dekker Inc.

Wadley HNG (2006). Multifunctional periodic cellular metals. Philosophical Transactions of The Royal Society A: Mathematical Physical and Engineering Sciences; 364 (1838): 31-68.

Wang AJ, McDowell DL (2004). In-Plane Stiffness and Yield Strength of Periodic Metal Honeycombs. Journal of Engineering Materials and Technology; 126(2): 137-156.

Wang AJ, Kumar RS, McDowell DL (2005). Mechanical behavior of extruded prismatic cellular metals. Mechanics of Advanced Materials and Structures; 12(3): 185-200.

Weibull WA (1939). A statistical theory of the strength of materials. Ingeniorsvetenscaps akademien Handlingar; 151: 1-29.

Wiedenhoeft AC, Miller RB (2005). Structure and function of wood. In: Handbook of wood chemistry and wood composites edited by Rowell RM. Boca Raton: CRC Press: 9-33.

Wiedenhoeft AC (2010). Structure and function of wood. In: Wood Handbook, Wood as an Engineering Material. Madison: U.S. Department of Agriculture, Forest Service, Forest Products Laboratory: 62-79.

Xiao Y, Kawai M, Hatta H (2011). An integrated method for off-axis tension and compression testing of unidirectional composites. Journal of Composite Materials; 45(6): 657-669.

Yang M, Huang J (2006). Failure surfaces for brittle honeycombs with Plateau borders under in-plane biaxial loads. Composite Structures; 72(4): 512-520.

Yin HF, Wen G, Gan N (2011). Crashworthiness design for honeycomb structures under uniaxial dynamic loading. International Journal of Computational Methods; 8: 863-877.

Zhu HX, Hobdell JR, Windle AH (2001). Effects of cell irregularity on the elastic properties of 2D Voronoi honeycombs. Journal of the Mechanics and Physics of Solids; 49(4): 857-870.

Publications

Aalto-DD 181/2013

ISBN 978-952-60-5421-6
ISBN 978-952-60-5422-3 (pdf)
ISSN-L 1799-4934
ISSN 1799-4934
ISSN 1799-4942 (pdf)

Aalto University
School of Engineering
Department of Applied Mechanics
www.aalto.fi

BUSINESS +
ECONOMY

ART +
DESIGN +
ARCHITECTURE

SCIENCE +
TECHNOLOGY

CROSSOVER

**DOCTORAL
DISSERTATIONS**